Am J Cancer Res 2021;11(5):2124-2141
www.ajcr.us /ISSN:2156-6976/ajcr0130566

Original Article

Exosomal transfer of miR-429 confers chemoresistance in epithelial ovarian cancer

Taoqiong Li[1,2*], Li Lin[1,2*], Qin Liu[4*], Wujiang Gao[1,2], Lu Chen[1,2], Chunli Sha[1,2], Qi Chen[2], Wenlin Xu[2], Yuefeng Li[3], Xiaolan Zhu[1,2,5]

[1]Reproductive Medicine Center, The Fourth Affiliated Hospital of Jiangsu University, Zhenjiang, Jiangsu, China; [2]Department of Central Laboratory, The Fourth Affiliated Hospital of Jiangsu University, Zhenjiang, China; [3]Department of Radiology, Affiliated Hospital of Jiangsu University, Zhenjiang, China; [4]Department of Obstetrics and Gynecology, The Kunshan Affiliated Hospital of Jiangsu University, Kunshan, China; [5]International Genome Center of Jiangsu University, Zhenjiang, China. [*]Equal contributors.

Received January 21, 2021; Accepted March 22, 2021; Epub May 15, 2021; Published May 30, 2021

Abstract: The development of multidrug resistance during chemotherapy is the main obstacle for epithelial ovarian cancer (EOC) treatment. Exosomal transfer of carcinogenic microRNAs (miRNAs) might strengthen chemoresistance in recipient cells. Here, we identified through microarray analysis higher miR-429 expression in multidrug-resistant SKOV3 cells and their secreted exosomes (SKOV3-EXO) than in sensitive A2780 cells and their secreted exosomes. SKOV3-derived exosomes were internalized by A2780 cells, which permitted the transfer of miR-429. Exosomal miR-429 enhanced the proliferation and drug resistance of A2780 cells by targeting calcium-sensing receptor (CASR)/STAT3 pathway in vitro and in vivo. In addition, NF-κB-p65 was predicted to bind to the miR-429 promoter region, and the inhibition of NF-κB reduced the expression of miR-429 and led to the sensitivity of EOC cells. Consistently, A2780 cells co-incubated with SKOV3 pretreated with an NF-κB inhibitor or miR-429 antagomir showed sensitivity to cisplatin and exhibited attenuated cell proliferation. Based on our data, exosomal miR-429 functions as a primary regulator of the chemoresistance and malignant phenotypes of EOC by targeting CASR through a mechanism promoted by NF-κB and might be a therapeutic target for EOC.

Keywords: Exosome, miR-429, chemoresistance, NF-κB, EOC

Introduction

Epithelial ovarian cancer (EOC) accounts for the vast majority of ovarian cancers (OCs) [1]. The emergence of drug resistance during chemotherapy is an important cause of treatment failure in patients with EOC, and the mechanism has not yet been elucidated [2, 3]. However, the acquisition of drug resistance not only occurs due to changes in the biological characteristics of the cell itself or repeated drug stimulation, as well as exogenous acceptance [4].

Exosomes are nano-scale microvesicles (30-100 nm in diameter) formed by the invagination of late endosomes released into the extracellular environment after fusion with the cell membrane [5, 6]. The lipid membrane facilitates the uptake of exosomes by contiguous alternately inaccessible beneficiary cells; then, after uptake, the substances in exosomes exert their biological functions, which are known as the third cell division correspondence method [7]. The cells that take up exosomes, including malignant cells, might obtain RNA cargo, particularly exosomal microRNAs (miRNAs), which have attracted considerable attention from researchers. Exosomal miRNAs are protected from digestion by RNases because of the lipid membranes. New evidence has described important roles for exosomal miRNAs (EXO-miRNAs) secreted by tumor cells in regulating tumor growth, angiogenesis, metastasis, and chemotherapy resistance [7-10]. Interestingly, recent studies have shown that drug-resistant cancer cells develop chemoresistance to recipient cells following EXO-miRNA transformation. For example, doxorubicin chemoresistance is conferred by the exosomal delivery of miR-501

in gastric cancer [11], and exosomal delivery of microRNA-32-5p leads to drug resistance in hepatocellular carcinoma [12]. Furthermore, exosomes secreted from resistant cells confer characteristics of the malignant phenotype through the transfer of miRNA-222-3p in non-small cell lung cancer (NSCLC) [13].

This study aimed to explore whether miRNAs are transferred via exosomes and the effects of these exosomal miRNAs on drug resistance in EOC cells in vitro and in vivo. We also aimed to investigate the underlying mechanisms and potential prognostic biomarkers for EOC.

Materials and methods

Patients

3 EOC patients treated in our department from January 2021 to February 2021 were included in this study. These patients provided serum samples prior to chemotherapy. Three serum samples from normal people (healthy volunteers) were also collected as a negative control group. All serum samples were stored at -80°C for future research. This study was carried out in accordance with the 1975 Declaration of Helsinki. The Research Ethics Committee of the Fourth Affiliated Hospital of Jiangsu University approved the study. Each patient's and healthy volunteer's identification number was encrypted to protect their privacy; thus, the need for informed consent was waived. The characteristics of NC and EOC patients were provided in Table S1.

Cell culture

The human EOC cell lines A2780 and SKOV3 were purchased from iCell Bioscience Inc. (Shanghai, China). The A2780 and SKOV3 cell lines were authenticated by the short tandem repeat assay (STR). The cell lines were cultured in RPMI 1640 medium containing 10% FBS (Thermo Fisher, Carlsbad, CA). For the coculture experiment, A2780 cells were grown in the upper chamber of a 0.4-μm-pore size Transwell insert and SKOV3 cells were plated in the lower chamber of the Transwell chamber. All cells were cultured in medium supplemented with 10% exosome-free FBS at 37°C in the presence of 5% CO_2.

Exosome isolation, quantification and labeling of cells

SKOV3 cells (1×10^6) were cultured in medium containing 10% exosome-free FBS for 48 h. Next, 40 ml of the conditioned medium was collected, and the collected supernatant was centrifuged at increasing speeds of 300×g for 10 min, 2000×g for 10 min, and 10,000×g at 4°C for 30 min to remove sediment and debris, thus obtaining pure exosomes. The supernatant was centrifuged at 100,000×g for 2 h to pellet the exosomes in clear ultracentrifuge tubes (Beckman Coulter, Indianapolis, USA). Transmission electron microscopy (TEM) was performed to verify the presence of exosomes. The exosomes were dissolved in PBS buffer, dropped onto a carbon-coated copper grid, and then stained with 2% uranyl acetate. The exosome images were obtained using an HT 7Tecnai G2 Spirit electron microscope (FEI Co, Oregon, USA). The exosomes were isolated from 40 ml of conditioned medium from SKOV3 cells by ultracentrifugation and then were resuspended in 100 μl of PBS. Before NTA, the SKOV3 cell-secreted exosomes were diluted by a factor of 100 with PBS to obtain an approximate number of vesicles of no more than 1×10^7. The size and concentration of the exosomes were analyzed using the ZetaView PMX 110 system (Particle Metrix, Meerbusch, Germany) and corresponding software (ZetaView 8.02.28). The exosomes from SKOV3 cells were labeled with PKH67 (Sigma-Aldrich, St. Louis, MO, USA) according to the manufacturer's instructions. The uptake of the labeled exosomes by A2780 cells was detected using a Leica TCS SP5 II laser scanning confocal microscope. GW4869 (Sigma-Aldrich, MO, USA) was utilized to block exosome formation and release at a concentration of 2.5 μM.

Exosomes isolation from patients serum

Frozen serum samples thawed in a 25°C water bath, completely thawed and placed on ice. Transfer serum to new tubes and centrifuged at 3000 g for 10 min at 4°C to remove cell debris. Transfer the supernatant to new tubes and centrifuged at 10,000 g for another 10 min at 4°C to remove impurities in the serum sample. Transfer the supernatant to new tubes and diluted 1:3 with pre-cooled PBS. Then add the same volume of Blood PureExo Solution (BPS,

Umibio, Shanghai, China) as the serum sample, and vibrated for 1 min. Stood for 2 hours at 4°C. Centrifuged at 10000 g for 60 min at 4°C to obtain the sediment riched exosomal particles, stored at -80°C for subsequent studies.

Transfection

SKOV3 cells and A2780 cells (3×10^5/well) were respectively transfected with mimic, inhibitor and the corresponding negative control (mimics-NC, inhibitor-NC) (GenePharma, Shanghai, China) of miR-429, miR-200b-5p and miR-1269b at 100 nM using Lipofectamine 2000. Cotransfection of 50 nM mir-429 inhibitor and 50 nM small siRNA specific for CASR (GenePharma, Shanghai, China) was also included.

RNA extraction and real-time quantitative RT-PCR (Qrt-PCR) analysis

Total RNA was extracted from exosomes, SKOV3 cells, A2780 cells, cocultured A2780 cells (CO-A2780), and frozen xenograft tumor tissues using TRIzol reagent (Invitrogen, CA, USA). qRT-PCR analysis for miR-429, miR-200b-5p and miR-1269b and CASR mRNA was performed according to the manufacturer's instructions. The relative expression of miR-429 was normalized to that of U6, and CASR mRNA expression was normalized to GAPDH; both were calculated using the 2 (-ΔΔCT) method.

Western blot analysis

Proteins from cells, xenograft tumors and serum exosomes were lysed in equal volumes of ice-cold lysis buffer and a protease inhibitor cocktail. The cell and xenograft tumor lysates were separated by SDS-PAGE and then transferred to a 0.2 μm PVDF membrane (Bio-Rad, USA). After blocking, the membranes were immunoblotted with CASR, stat3, p-stat3, NF-κB, (1:1000; Abcam, Cambridge, MA) primary antibodies and then with horseradish peroxidase-conjugated secondary antibodies (dilution 1:5000). GAPDH (1:5000; Abcam, Cambridge, MA) was used as an endogenous control. The Odyssey Infrared Imaging System was used to visualize the targeted protein bands.

Apoptosis assay

Flow cytometry analysis was performed using the Annexin V-APC/7AAD Apoptosis Detection Kit (KeyGen BioTech, Jiangsu, China) according to the manufacturer's instructions. Briefly, the cells were washed twice with cold PBS and then resuspended in 100 μl of 1× Binding Buffer, followed by the addition of 5 μl of Annexin V-APC and 5 μl of 7AAD and incubation for 15 min at room temperature in the dark. Thereafter, the cells were incubated with 400 μl of 1× Binding Buffer and analyzed by FACS Canto II flow cytometry (BD Biosciences).

RIP assay

The RIP assay was conducted using the RiboCluster Profiler RIP Assay Kit (MBL Medical & Biological Laboratories Co., Ltd., Japan) according to the manufacturer's instructions. The cells (1×10^7) were lysed in RIP lysis buffer containing protease inhibitors and an RNase inhibitor. Protein A/G magnetic beads were incubated with a CASR antibody (Abcam) or NC rabbit IgG overnight at 4°C. The precipitated RNAs were separated with TRIzol reagent, reverse transcribed using the Revert Aid Kit (Thermo) and subsequently detected with qPCR. All the samples were detected in triplicate using independent tests.

Mouse xenograft tumor model

Thirty 6-week-old female BALB/c nude mice were purchased from the Shanghai SLAC Laboratory Animal Co, Ltd. (Shanghai, China) and housed under specific pathogen-free (SPF) conditions. All animal experiments were conducted according to the guidelines of the Medical Laboratory Animal Health Committee of Jiangsu University. Mice were injected subcutaneously with A2780 cells (1.0×10^7) and randomly divided into 5 groups (n = 6 mice per group). We measured the volumes of the subcutaneous tumors in nude mice once every 2 days. SKOV3 cells were transfected with the miR-429 agomir or antagomir. When the volume of the xenografts reached approximately 50 mm^3, SKOV3 exosomes (50 μg) or PBS were intratumorally injected into the xenograft tumors three times a week for one week. All groups were then administered cisplatin (DDP, 5 mg/kg) three times a week for two weeks. On day 35, the mice in all groups were sacrificed, and tumors were harvested and frozen in liquid nitrogen.

Immunohistochemistry

Xenograft tumors were fixed in 4% PFA and embedded in paraffin wax. The tumor tissues

were sectioned at 4-μm thickness, dewaxed in gradient alcohol and xylene, and incubated with the primary antibodies KI-67 and CASR (both from Abcam, Cambridge, UK) for 12 h at 4°C in a humid environment. The sections were then incubated with a biotinylated secondary antibody for 1 h at 37°C.

ChIP assay

Chromatin immunoprecipitation (ChIP) ChIP assays were conducted with the SimpleChIP™ ENZYMATIC Chromatin IP Kit (Magnetic Beads, #90003, CST, US) according to the manufacturer's guidelines. Immunoselection of cross-linked protein-DNA was performed using the anti-NF-kB-P65 antibody and magnetic beads at 4°C overnight. Anti-rabbit IgG was used as a negative control. The purified DNAs were analyzed using qRT-PCR. The forward and reverse primers sequences of p65-chip-343, p65-chip-283, p65-chip-242 for the hsa-miR-429 promoter were provided in Table S7.

Statistical analysis

Statistical analyses were conducted using SPSS software. At least three biological replicates were performed in each experiment in our study, and the data are presented as the means ± SD. The statistical significance of differences between two groups was assessed using two-tailed Student's t test. One-way ANOVA was adopted to compare the means among multiple groups. *P < 0.05, **P < 0.01, AND ***P < 0.001.

Results

The cisplatin (DDP) resistance of A2780 cells is enhanced after coculture with SKOV3 cells

The half-maximal inhibitory concentrations (IC50s) of cisplatin (DDP), paclitaxel (PTX) and cytoxan (CTX) were increased in SKOV3 cells compared with A2780 cells (**Figure 1A**), indicating that A2780 cells are more sensitive to DDP, PTX and CTX than SKOV3 cells. A2780 cells were cocultured with SKOV3 cells to determine the effects of SKOV3 cells on the DDP resistance of A2780 cells (**Figure 1B**). As expected, after coculture with SKOV3 cells, A2780 cells exhibited increased cell viability, enhanced drug resistance and a reduced apoptosis rate (**Figure 1C-F**). Based on these data, the drug resistance of A2780 cells was enhanced by SKOV3 cells.

SKOV3-secreted exosomes confer chemoresistance to recipient A2780 cells

We isolate exosomes from the conditioned medium of SKOV3 cells to explore the roles of exosomal delivery in DDP resistance. The double-layered vesicles displayed a round shape with a diameter ranging from 50 nm to 200 nm under TEM (**Figure 2A**). The Nanosight particle tracking analysis (NTA) further confirmed that the size of most vesicles was 80 nm after multiple dilutions (**Figure 2B**). The exosomal markers CD63 and CD81 were detected in the exosomes using a flow cytometry analysis (**Figure 2C**). Thus, the vesicles secreted from SKOV3 cells display typical characteristics of exosomes.

Next, we used the fluorescent tracer PKH67 to label SKOV3-EXO and visualize exosomal delivery. After incubating the labeled SKOV3-EXO with A2780 cells, strong green fluorescence was observed in the cytoplasm of the recipient cells (A2780 cells) with a confocal microscope (**Figure 2D**, **2E**), suggesting that the recipient A2780 cells successfully absorbed the exosomes derived from SKOV3 cells.

GW4869 was employed to prevent exosome secretion from SKOV3 cells plated in the lower chamber of a coculture system with 0.4-μm pores (Corning. American), and A2780 cells were plated in the upper chamber and collected for subsequent experiments to further determine whether the transfer of drug resistance from SKOV3 cells to A2780 cells depend on exosomes (**Figure 1B**). The viability and DDP resistance of A2780 cells were decreased upon coculture with SKOV3 cells pretreated with GW4869. Next, SKOV3-EXO was directly added to the medium of A2780 cells (A2780 + SKOV3-EXO). The CCK8 assay showed an increase in the viability of A2780 cells treated with SKOV3-EXO. The IC50 of DDP was increased in A2780 cells incubated with SKOV3-EXO compared with A2780 cells cocultured with an equal amount of PBS (**Figure 2F**, **2G**). In summary, these results revealed that exosomes secreted from the drug-resistant EOC cells were transferred to the adjacent drug-sensitive EOC cells, thus conferring chemoresistance to DDP.

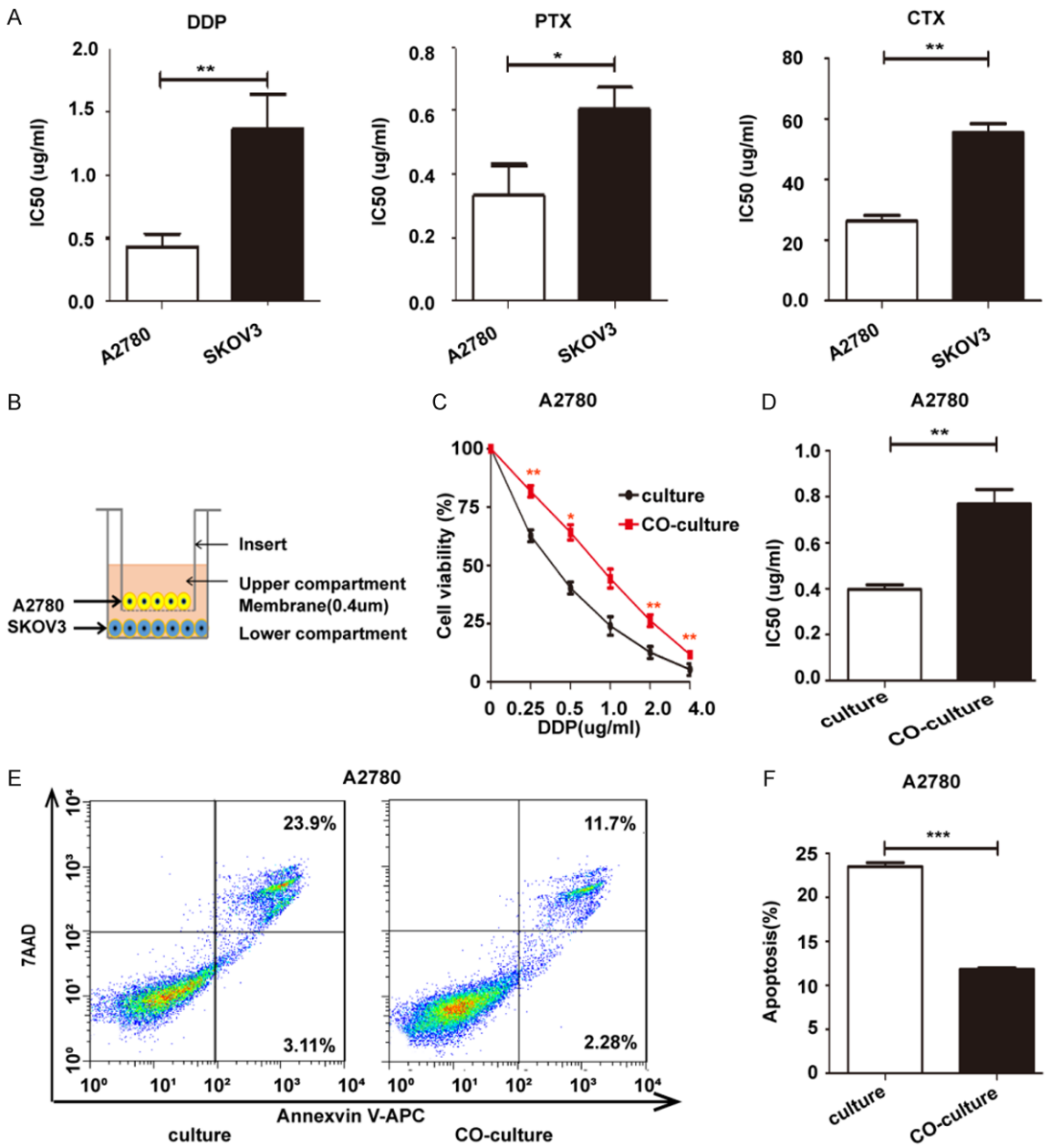

Figure 1. Drug resistance identification and the resistance effect of SKOV3 cells on A2780 cells. (A) IC50 for DDP, PTX and CTX in SKOV3 cells and A2780 cells. (B) Schematic diagram of coculture. Cell viability (C) and IC50s for DDP (D) of A2780 cells and A2780 cells cocultured with SKOV3 cells. Apoptosis (E) and the related quantitative analysis of apoptosis (F) of A2780 cells and A2780 cells cocultured with SKOV3 cells.

Identification and screening of differentially expressed miRNAs in A2780 cells compared with SKOV3 cells and A2780-EXO compared with SKOV3-EXO

We detected the expression profile of microRNAs in A2780 compared with SKOV3 cells and A2780-EXO compared with SKOV3-EXO using next-generation sequencing (NGS) (Guangzhou RiboBio Co., Ltd.) to evaluate the role of exosomal miRNAs in the drug resistance mechanism of EOC cells. The original sequencing data was provided in the supplementary material. Significant differentially expressed miRNAs were selected based on log2 (fold change) ≥10. The heatmap showed higher expression of 16 miRNAs and lower expression of 17 miRNAs in SKOV3 cells than in A2780 cells (**Figure 3A**, left

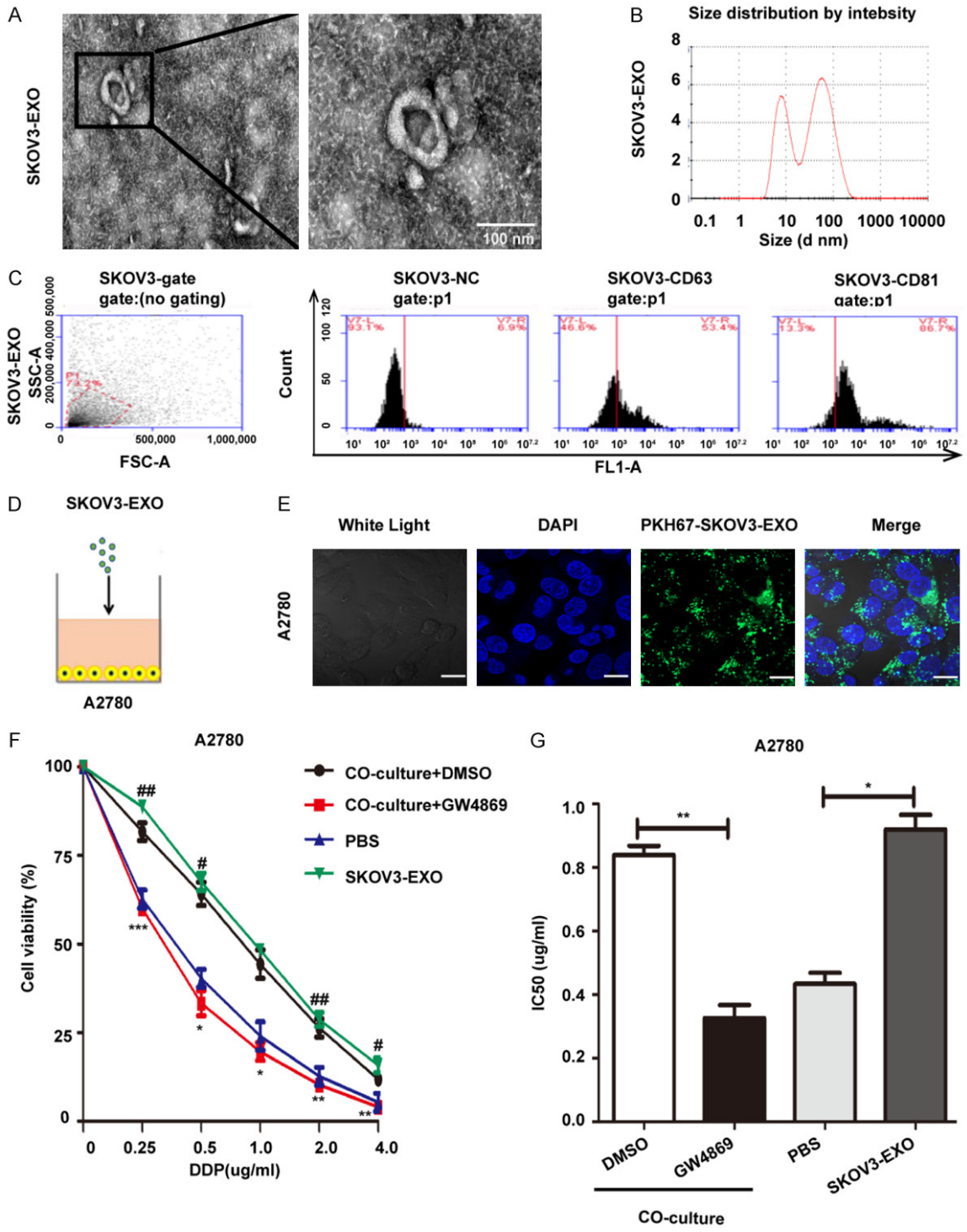

Figure 2. SKOV3 cells enhance the chemoresistance of A2780 recipient cell exosomes. (A) Transmission electron micrography showed round-shaped vesicles with bilayered membranes ranging from 50 nm to 200 nm in diameter released by SKOV3 (SKOV3-EXO). Scale bar: 100 nm. (B) Nanosight particle tracking analysis (NTA) indicated that the dominant size of SKOV3-EXO was approximately 100 nm. (C) FCM analysis of exosomal marker proteins CD63 and CD81 in SKOV3-EXO. (D) Schematic diagram of A2780 cells cocultured with SKOV3-EXO. (E) Confocal microscopy showed exosome internalization by A2780 recipient cells after coincubation with PKH67-labeled (green fluorescence) SKOV3-EXO. DAPI was used to stain the nuclei of A2780 recipient cells with blue fluorescence. Scale bar = 10 μm. Cell viability (#: PBS vs SKOV3-EXO, *: CO-culture+DMSO vs CO-culture+GW4869) (F) and IC50s for DDP (G) of cocultured A2780+DMSO, cocultured A2780+GW4869, A2780+PBS, and A2780+SKOV3-EXO.

panel). The heatmap also showed higher expression of 15 miRNAs and lower expression of 2 miRNAs in SKOV3-EXO than in A2780-EXO (**Figure 3A**, right panel). Next, the Venn diagram revealed three miRNAs (miR-429, miR-200b-5p and miR-1269b) with higher expression in both comparison groups (**Figure 3B**). We used RT-PCR to verify the expression of the upregulated miRNAs mentioned above. Nine miRNAs were expressed at higher levels in SKOV3 cells than in A2780 cells, and 5 miRNAs were expressed at higher levels in SKOV3-EXO than in A2780-EXO. Three miRNAs (miR-429, miR-200b-5p and miR-1269b) displayed higher expression in both comparison groups, consistent with the NGS results. (The results of the PCR verification of the three miRNAs are shown in **Figure 3C**; the results of the verification of other miRNAs are presented in Figure S1). Based on these results, three miRNAs may serve as potential messengers of drug resistance information and play important roles in the drug resistance of EOC. The three miRNAs had higher expression in SKOV3 than A2780 in both cell and exosomes. The expression difference of miR-429 in SKOV3-EXO and A2780-EXO was the most obvious. And in clinical samples, the expression of miR-429 in exosomes from peripheral blood of ovarian cancer also increased significantly, compared to normal people Figure S2.

The effect of miR-429 on the chemoresistance of A2780 cells is mediated by targeting CASR

According to the NGS results, three miRNAs (miR-429, miR-200b-5p and miR-1269b) were highly related to chemoresistance in EOC cells. A2780 cells (3×10^5/well) were transfected with the agomirs of miR-429, miR-200b-5p or miR-1269b or with agomir-NC at 100 nM to explore the functions of these miRNAs in drug resistance. A2780 cells transfected with miR-429-agomir showed a higher IC50 than A2780 cells transfected with miR-200b-5p-agomir or miR-1269b-agomir (**Figure 4A**). Hence, miR-429 had the strongest contribution to drug resistance. Thereafter, we verified whether miR-429 was delivered by exosomes. SKOV3 cells transfected with Cy3-miR-429 mimic were plated in the lower chamber of the coculture system. After 48 hours of cocultivation, the A2780 cells inoculated in the upper chamber displayed strong red fluorescence (**Figure 4B**). Therefore, miR-429 may be delivered from SKOV3 cells to A2780 cells by exosomes. A2780 cells (3×10^5/well) were transfected with the agomir, antagomir or the negative control (agomir-NC or antagomir-NC) of miR-429 at 100 nM (chosen for transfected cell lines substantiated by qRT-PCR, Figure S3A) to further determine the effect of miR-429 on the chemoresistance of A2780 cells. A2780 cells transfected with the agomir showed increased drug resistance, and A2780 cells transfected with the antagomir were much more sensitive to DDP (**Figure 4C**). These results indicate that miR-429 overexpression contributed to drug resistance in vitro.

Notably, miRNAs to the 3'-untranslated region (3'-UTR) of the target mRNA to directly degrade the mRNA or inhibit post-transcriptional protein translation and negatively regulate gene expression [14-16]. The selected target genes of miR-429 were predicted by TargetScan, miRanda, and miRWalk. Since these programs have a certain false positive rate, only the genes predicted by all three programs were proposed to be miRNA target genes. One hundred eighty-six genes were predicted to be targeted by miR-429 (Table S2). One miRNA may regulate the expression of multiple target genes, and the one gene might also be targeted by several miRNAs [17, 18]. According to the results of target gene prediction, calcium-sensing receptor (CASR) showed the highest align_score in miRanda, 4 binding sites in CASR were predicted by miRWalk, all with binding probabilities of 100%, and the site type of CASR was 8mer-1a in TargetScan (Figure S3B; Tables S3, S4, S5). In summary, CASR was identified by the three target gene prediction websites and showed a good score. Additionally, CASR was confirmed to be associated with chemotherapy resistance in colon cancer and breast cancer [19-21]. After considering these findings, we chose CASR as the target gene for subsequent study. We detected the changes in the CASR mRNA and protein levels in A2780 cells transfected with the agomir and antagomir to assess the effect of miR-429 on CASR expression. The levels of the CASR mRNA and the proteins expression of CASR were attenuated in the agomir group and elevated in the antagomir group; the expression of stat3 and p-stat3 were elevated in the agomir group and attenuated in the antagomir group (**Figure 4D**, **4E**). RIP assays were conducted in A2780 cells using the IgG antibody, followed by qRT-PCR analysis of miR-429 in immunoprecipitated

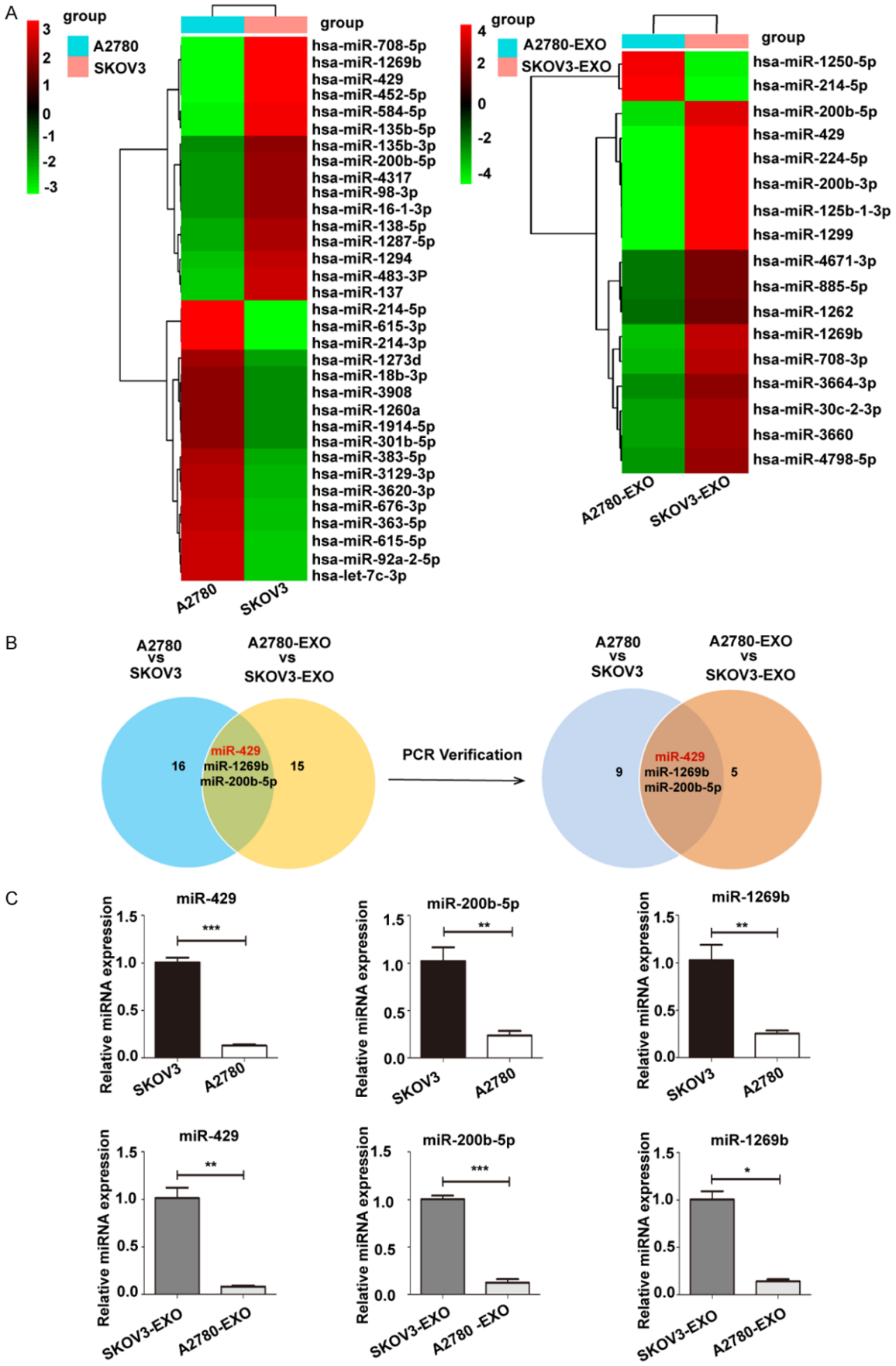
A
group
A2780
SKOV3
hsa-miR-708-5p
hsa-miR-1269b
hsa-miR-429
hsa-miR-452-5p
hsa-miR-584-5p
hsa-miR-135b-5p
hsa-miR-135b-3p
hsa-miR-200b-5p
hsa-miR-4317
hsa-miR-98-3p
hsa-miR-16-1-3p
hsa-miR-138-5p
hsa-miR-1287-5p
hsa-miR-1294
hsa-miR-483-3P
hsa-miR-137
hsa-miR-214-5p
hsa-miR-615-3p
hsa-miR-214-3p
hsa-miR-1273d
hsa-miR-18b-3p
hsa-miR-3908
hsa-miR-1260a
hsa-miR-1914-5p
hsa-miR-301b-5p
hsa-miR-383-5p
hsa-miR-3129-3p
hsa-miR-3620-3p
hsa-miR-676-3p
hsa-miR-363-5p
hsa-miR-615-5p
hsa-miR-92a-2-5p
hsa-let-7c-3p
A2780
SKOV3
group
A2780-EXO
SKOV3-EXO
hsa-miR-1250-5p
hsa-miR-214-5p
hsa-miR-200b-5p
hsa-miR-429
hsa-miR-224-5p
hsa-miR-200b-3p
hsa-miR-125b-1-3p
hsa-miR-1299
hsa-miR-4671-3p
hsa-miR-885-5p
hsa-miR-1262
hsa-miR-1269b
hsa-miR-708-3p
hsa-miR-3664-3p
hsa-miR-30c-2-3p
hsa-miR-3660
hsa-miR-4798-5p
A2780-EXO
SKOV3-EXO
B
A2780 vs SKOV3
A2780-EXO vs SKOV3-EXO
16
miR-429
miR-1269b
miR-200b-5p
15
PCR Verification
A2780 vs SKOV3
A2780-EXO vs SKOV3-EXO
9
miR-429
miR-1269b
miR-200b-5p
5
C
miR-429
Relative miRNA expression
SKOV3
A2780
miR-200b-5p
miR-1269b
SKOV3-EXO
A2780-EXO
A2780 -EXO

Figure 3. Identification and screening of miRNAs in A2780 cells vs SKOV3 cells and A2780-EXO vs SKOV3-EXO. A. The heatmap showed that 16 miRNAs have higher expression levels and 17 miRNAs have lower expression levels in SKOV3 cells than in A2780 cells (left panel); 15 miRNAs have higher expression levels and 2 miRNAs have lower expression levels in SKOV3-EXO compared with those in A2780-EXO (right panel). B. The Venn diagram shows three miRNAs (miR-429, miR-200b-5p and miR-1269b) with higher expression in both comparison groups. C. Real-time qRT-PCR revealed that the levels of miR-429, miR-200b-5p and miR-1269b were higher in SKOV3 cells than in A2780 cells and that the levels were higher in SKOV3-EXO than in A2780-EXO.

RNAs to further confirm the relationship between CASR and miR-429. The RIP results indicated that miR-429 was enriched in the RNA immunoprecipitate using the anti-CASR antibody compared to IgG (**Figure 4F**), supporting the hypothesis that CASR interacts with miR-429 in A2780 cells. Then, we inhibited CASR expression on the basis of the miR-429 antagomir transfection. The inhibition of CASR could largely rescue the increase in CASR expression level and the decrease in drug resistance via stat3 pathway caused by miR-429 antagomir (**Figure 4G**, **4H**) (The infection efficiency of si-CASR was confirmed by Western blot analyses in Figure S3D, the original uncropped gels of Western blot assay was shown in Figure S7). These data further verified that miR-429 conferred DDP resistance to A2780 cells via CASR/ STAT3 pathway.

Exosomal miR-429 induces drug resistance in EOC in vivo via CASR/STAT3 pathway

We subcutaneously injected A2780 cells into female mice to produce appropriately sized tumors and study the function of miR-429 present in SKOV3-EXO in tumor growth and chemoresistance. Exosomes (50 μg) (Figure S4) or PBS were injected into the xenograft tumors three times a week for one week (n = 6). We provide a simple flow chart of the animal experiments in **Figure 5A**. Xenografts injected with miR-429-overexpressing SKOV3-EXO grew significantly larger. In contrast, miR-429 inhibition abrogated SKOV3-EXO-regulated tumor growth in mice (**Figure 5B**, **5C**). We quantified the expression of CASR and a tumor cell proliferation marker (KI67). Xenografts injected with miR-429-overexpressing SKOV3-EXO displayed a remarkable increase in the numbers of KI67-positive (KI67+) cells and decreased CASR expression (**Figure 5D**). Xenografts injected with miR-429-overexpressing SKOV3-EXO showed higher miR-429 expression, lower CASR expression and higher p- STAT3 expression (**Figure 5E**, **5F**). A reduced number of KI67 + cells, a decrease in miR-429 expression, an increase in CASR expression and a decrease p-STAT3 expression were observed in xenografts treated with exosomes containing the miR-429 inhibitor. These results further support the hypothesis that the exosomal transfer of miR-429 downregulated CASR and impaired the therapeutic effects of DDP in vivo.

Exosomal miR-429 promoted by NF-κB functions as a principal regulator of drug resistance and the malignant characteristics of EOC

Because increased miR-429 expression caused drug resistance, we sought to identify factors that might affect miR-429 expression using a transcription factor prediction website. Many transcription factors were involved in the transcription of miR-429. We predicted the transcription factors regulating miR-429 using the TRANSFAC 8.3 database according to the sequence of the miR-429 promoter region (2000 bp upstream and 1 bp upstream). We have provided the transcription factor prediction results for miR-429 in Table S6. According to the prediction, we found that there were three NF-κB binding sites in the promoter region of miR-429 with high specificity. NF-κB was associated with the resistance of various tumors. Therefore, we predicted that NF-κB might be the transcription factor regulating miR-429. Then we detected the effect of NF-κB on miR-429 expression. We treated SKOV3 and A2780 cells with gradient concentrations of the NF-κB inhibitor PDTC. Notably, miR-429 was downregulated in SKOV3 and A2780 cells treated with increased concentrations of PDTC, according to our tests (**Figure 6A**, **6B**). Furthermore, we conducted experiments to explore the effect of NF-κB on the drug resistance of EOC. After treatment with 200 μM PDTC, the viability and IC50 of SKOV3 and A2780 cells were both decreased (**Figure 6C**, **6D**). Based on these results, NF-κB promoted drug resistance in ovarian cancer (OC). Next, we cocultured A2780 cells with PDTC-treated SKOV3 cells to determine whether the regula-

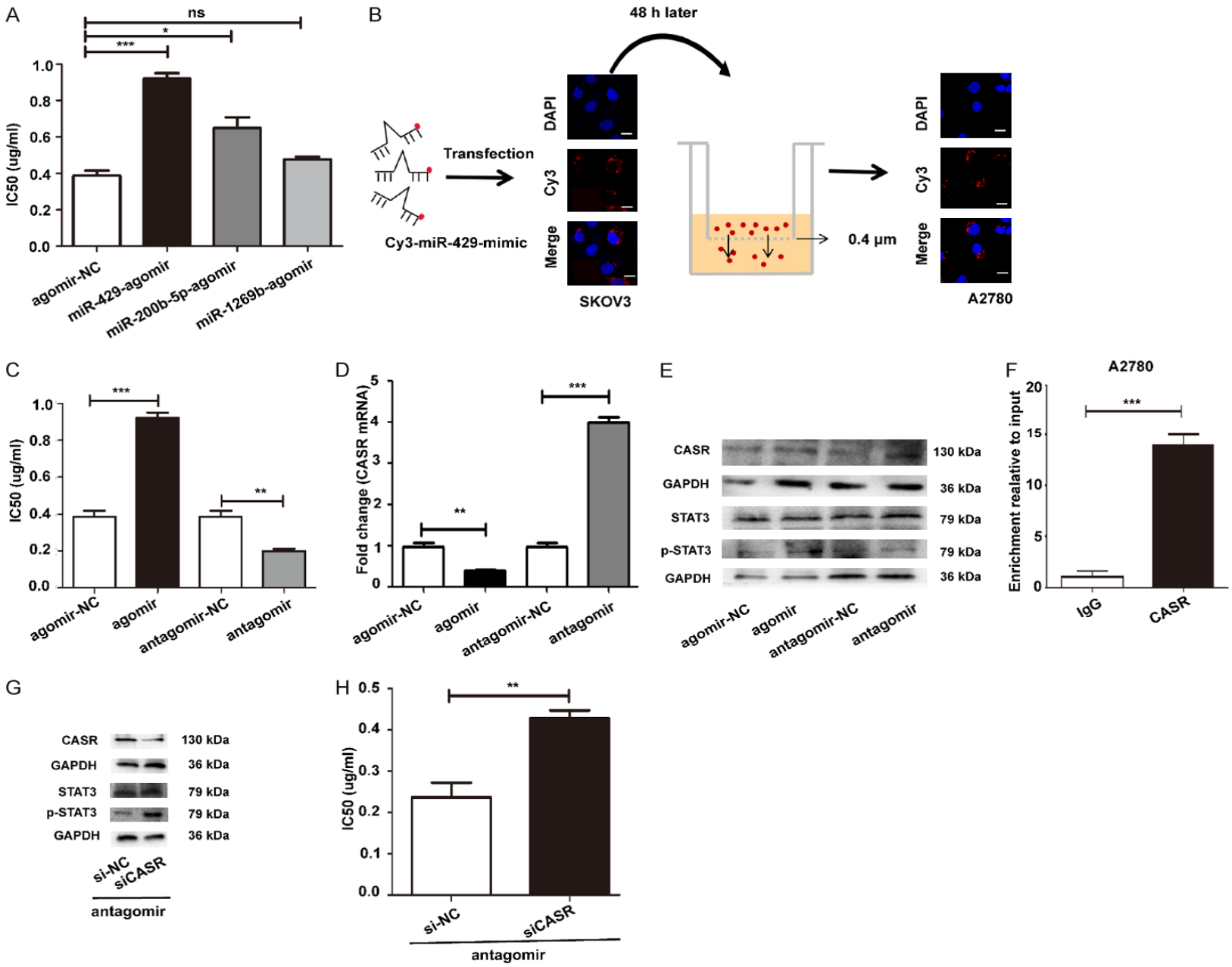
A
ns
*
***
IC50 (ug/ml)
agomir-NC
miR-429-agomir
miR-200b-5p-agomir
miR-1269b-agomir
B
48 h later
Transfection
Cy3-miR-429-mimic
DAPI
Cy3
Merge
SKOV3
0.4 μm
A2780
C
agomir-NC
agomir
antagomir-NC
antagomir
D
Fold change (CASR mRNA)
E
CASR
GAPDH
STAT3
p-STAT3
130 kDa
36 kDa
79 kDa
F
A2780
Enrichment realative to input
IgG
CASR
G
si-NC
siCASR
antagomir
H

Figure 4. Chemoresistant effect of miR-429 on A2780 cells by CASR/STAT3 pathway. (A) After transfection with the agomirs of miR-429, miR-200b-5p and miR-1269b, the A2780 cells were treated with different concentrations of DDP for 48 h. DDP resistance was significantly enhanced in A2780 miR-429 agomir cells compared with that in A2780 miR-200b-5p agomir cells and A2780 miR-1269b agomir cells. (B) SKOV3 cells transfected with the Cy3-miR-429 mimic (red fluorescence) were plated in the lower chamber and coincubated with A2780 cells seeded in the upper chamber in a coculture system with a 0.4-μm pore membrane. Red fluorescence was observed in the A2780 recipient cells under the fluorescence microscope. Scale bar = 10 μm. IC50 for DDP (C), fold change of CASR mRNA (D) and CASR, STAT3, p-STAT3 protein levels (E) in A2780 miR-429 agomir, A2780 miR-429 agomir NC, A2780 miR-429 antagomir, and A2780 miR-429 antagomir NC. (F) RIP assays using an anti-CASR antibody showed that CASR interacts with miR-429 in A2780 cells, followed by qRT-PCR analysis of miR-429 in immunoprecipitated RNAs. The CASR, STAT3, p-STAT3 protein levels (G) (The original uncropped gels of Western blot assay were shown in Figure S6) and IC50s for DDP (H) of A2780 miR-429 antagomir NC, A2780 miR-429 antagomir, A2780 miR-429 antagomir+siCASR-NC, A2780 miR-429 antagomir+siCASR.

tory effect of NF-κB on EOC resistance was related to miR-429. The viability and IC50 of A2780 cells decreased compared with A2780 cells cocultured with SKOV3 cells (**Figure 6E**). The viability and IC50 of A2780 cells were also attenuated upon coculture with SKOV3-antagomir-treated SKOV3 cells (**Figure 6F**). These data further illustrate that NF-κB promotes drug resistance and may be related to miR-429 expression. According to the results of the ChIP-qPCR assay in SKOV3 and A2780 cells, p65-chip-343, p65-chip-283, p65-chip-242 could bound to miR-429 promoter and the enrichment efficiency of p65-chip-343 was more than 10 fold changes (**Figure 6G**).

Based on these results, we proposed a model for the underlying effects of exosomal miR-429 on EOC (the schematic diagram was presented in Figure S5). SKOV3 cell-derived exosomes containing miR-429 were taken up by the recipient cells and enhanced drug resistance. NF-κB may increase drug resistance by promoting miR-429 transcription.

Discussion

Platinum-based therapy is the main treatment option for OC, while chemoresistance often leads to therapeutic failure [22, 23]. Exosomes have been reported to play an important role in chemoresistance as novel intracellular communication molecules [24-26]. Recently, miRNAs were observed to be loaded in exosomes to escape degradation [27]. These exosomal miRNAs are shuttled into the recipient cells and change the phenotype of these cells by promoting changes in gene expression [28, 29]. Chemotherapy-resistant tumor cells may release exosomal miRNAs to the microenvironment and endow the recipient cells with drug resistance [30-32]. As shown in the study by Wang et al., the exosomal transfer of miR-155-5p from the paclitaxel-resistant MGC-803 gastric cancer cells promoted the EMT and drug resistance in paclitaxel-sensitive cells [33]. Exosomes decrease the adriamycin sensitivity of breast cancer cells by transferring miRNAs [8].

We identified the differentially expressed miRNAs in drug-resistant and drug-sensitive cells and their secreted exosomes by performing a microarray analysis to detect the messengers of drug resistance information in OC. Significant differentially expressed miRNAs were selected based on log2 (fold change) ≥10. After qRT-PCR identification, we discovered 9 miRNAs with higher expression levels in SKOV3 cells than in A2780 cells, and 5 miRNAs displayed higher expression levels in SKOV3-EXO than in A2780-EXO, as shown in the heatmap. Higher expression of miR-429 was detected in SKOV3 cells than in A2780 cells, and miR-429 was expressed at significantly higher levels in SKOV3-EXO than in A2780-EXO. SKOV3-EXO were taken up by recipient cells and maintained their effects, suggesting that miR-429 may be appropriate for packaging into exosomes to retain its stability and subsequently play a significant role in chemoresistance. In our study, high expression of miR-429 increased cell viability and drug resistance. Based on accumulating evidence, miR-429 dysregulation is related to the EMT, progression, development, invasion, metastasis, apoptosis and drug resistance of various cancers [34]. Combined with the results of NGS and assessments of cellular function, we selected miR-429 as the candidate miRNA. Notably, miR-429 belongs to the miR-200 family, which includes miR-200a, miR-200b, miR-200c, miR-141 and miR-429 and is located on chromosome 1 [35]. Previous studies have reported negative correlations between the miR-429 expression level and renal cell carcinoma (RCC) [36], breast cancer (BC) [37], gastric carcinoma (GC) [38], glioblastoma (GBM)

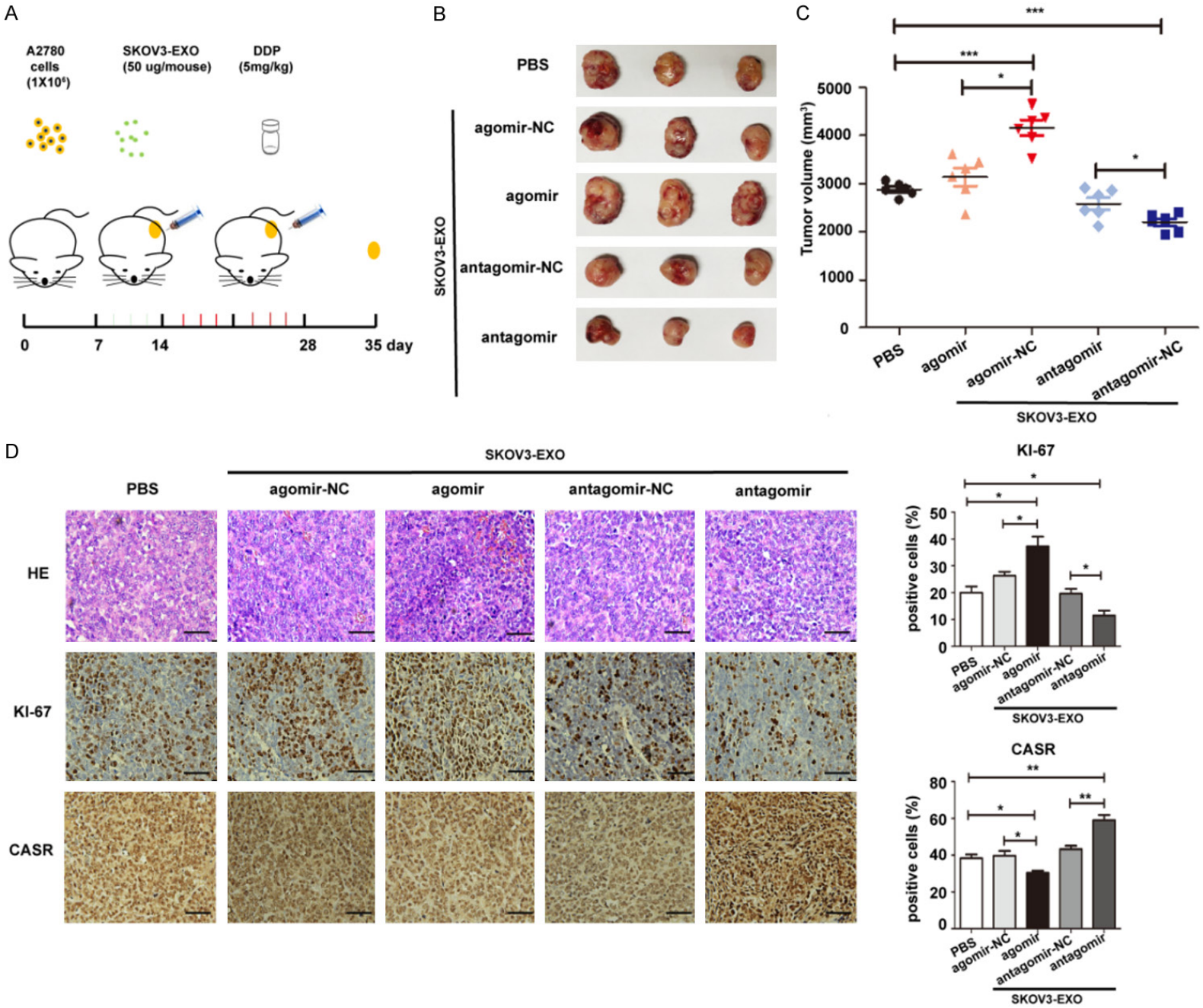
A
A2780 cells (1X10⁶)
SKOV3-EXO (50 ug/mouse)
DDP (5mg/kg)
0
7
14
28
35 day
B
PBS
agomir-NC
agomir
antagomir-NC
antagomir
SKOV3-EXO
C
Tumor volume (mm³)
5000
4000
3000
2000
1000
0
PBS
agomir
agomir-NC
antagomir
antagomir-NC
SKOV3-EXO
D
SKOV3-EXO
PBS
agomir-NC
agomir
antagomir-NC
antagomir
HE
KI-67
CASR
KI-67
positive cells (%)
CASR
positive cells (%)

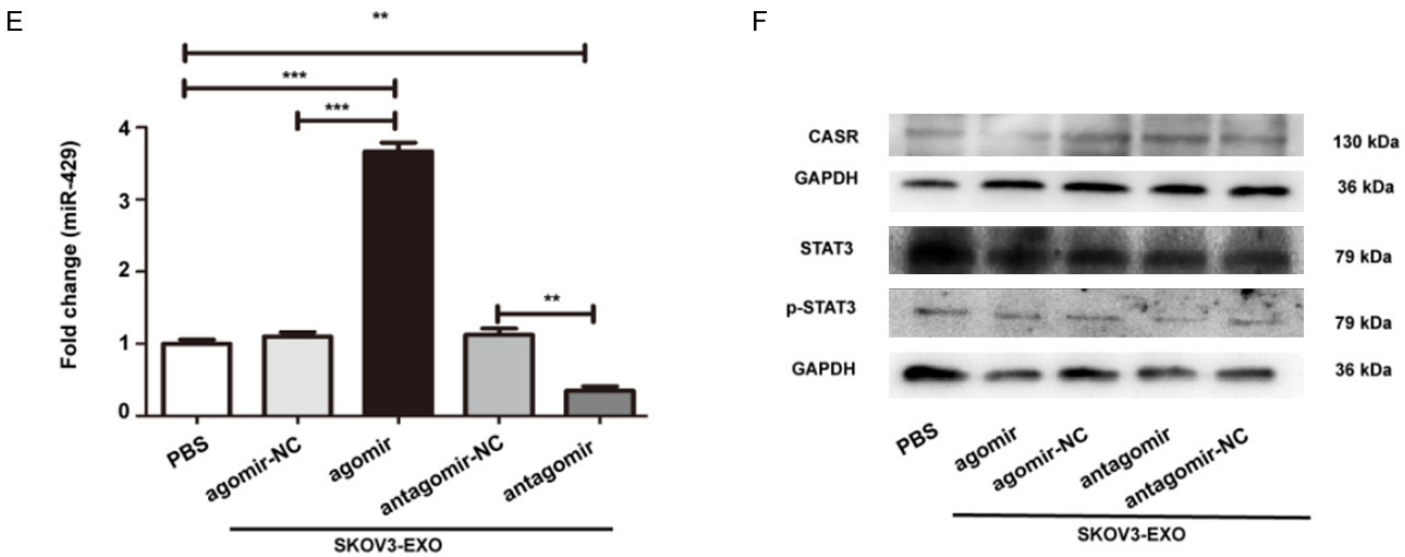

Figure 5. Effect of exosomal miR-429 in DDP resistance in vivo. Exosomes derived from SKOV3 cells were transfected with agomir or antagomir (SKOV3-EXO-agomir-NC, SKOV3-EXO-agomir, SKOV3-EXO-antagomir-NC, and SKOV3-EXO-antagomir). A2780 cells were subcutaneously injected into BALB/c nude mice, and potential tumors were allowed to grow for a week. Next, exosomes (50 μg) or PBS was intratumorally injected into the xenograft tumors three times per week for one week (n = 6). All the groups were administered DDP (5 mg/kg) by intraperitoneal injection three times a week for 2 weeks and were sacrificed. A. Flow chart of the animal experiment. B. Representative images of the excised tumors on day 35 after tumor cell injection. C. Tumor volumes of the excised tumors on day 35 after tumor cell injection. D. Immunohistochemistry analyses for KI-67 and CASR staining were carried out on A2780 xenograft tumor sections. Representative staining is shown (×200 magnification). E. The expression of miR-429 was higher in A2780+SKOV3-EXO-agomir cells than in A2780+PBS cells. The expression of miR-429 was lower in A2780+SKOV3-EXO-antagomir cells than in A2780+PBS cells. F. The level of CASR, STAT3, p-STAT3 proteins were downregulated in the A2780+SKOV3-EXO-agomir group, and the level of CASR protein was upregulated in the A2780+SKOV3-EXO-antagomir group, as assessed by Western blotting in mouse xenograft tumor tissues. The original uncropped gels of Western blot assay was shown in Figure S6. *P < 0.05 and **P < 0.01. ***P < 0.001.

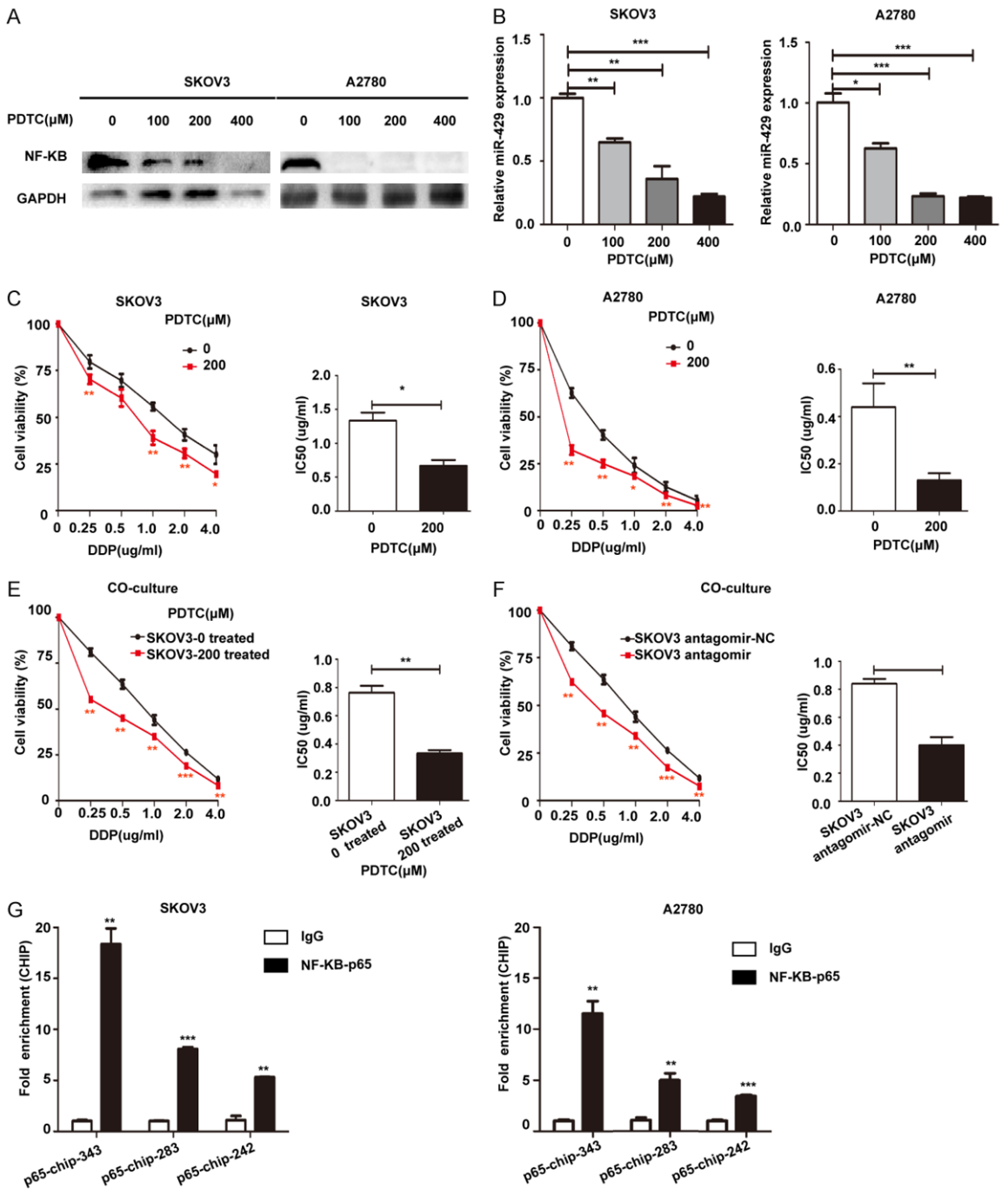

Figure 6. NF-κB promotes the transcription of miR-429 to mediate drug resistance. After treatment with different concentrations of PDTC for 24 h, NF-κB p65 protein expression in SKOV3 and A2780 cells were measured by Western blotting (A). The original uncropped gels of Western blot assay were shown in Figure S7. Additionally, the expression of miR-429 was detected by real-time qRT-PCR (B). Cell viability and IC50s for DDP of SKOV3 cells (C) and A2780 cells (D) treated with 0 or 200 μM PDTC (E). Cell viability and IC50s for DDP of A2780 cells cocultured with SKOV3 cells treated with 0 or 200 μM PDTC (F). Cell viability and IC50s for DDP of A2780 cells cocultured with SKOV3 transfected with miR-429 antagomir. The chrome immunoprecipitations (CHIP) were performed by using specific anti-NF-κB-p65 (G).

[39], esophageal cancer (EC) [40], osteosarcoma [41], and cervical cancer (CC) [42], and miR-429 is a negative indicator of the drug resistance of these cancer types. The potential explanation is that miR-429 is relevant to tumorigenesis in a specific pattern, which may

function as a tumor suppressor or promote the expression of certain cancer candidate genes in specific types of tumor cells/tissues. Moreover, the ability of miR-429 to enhance drug resistance was also consistent with previous research showing that miR-429 increased endometrial carcinoma, prostate cancer and lung cancer cell resistance. However, However, the functions of exosomal miR-429 in the chemoresistance of EOC remain to be elucidated [35].

In the present study, exosomal miR-429 released from SKOV3 cells was internalized by recipient cells. Exosomal miR-429 uptake increased the DDP resistance of recipient cells in vitro and in vivo, and exosomal miR-429 may function by targeting CASR. According to the GEPIA database (Figure S3C), the expression of CASR in OC was higher than in normal tissues. CASR was a class-CG protein-coupled receptor that played a key role in the process of calcium transformation, mainly regulating the secretion of parathyroid hormone to maintain systemic calcium homeostasis [19]. CASR promoted and maintained the malignant and drug-resistant phenotype of colon cancer and was a robust promoter of colonic epithelial cell differentiation that functions as a tumor suppressor in colon cancer. CASR also exerted anti-tumor effects on breast cancer and promotes the sensitivity of cells to cytotoxic drugs [21]. Hence, the CASR gene may be a novel potential tumor suppressor. Through a series of analyses, including qRT-PCR, Western blotting and RIP, miR-429 was confirmed to suppress CASR expression in A2780 cells. Previous studies reported that CASR was involved in cardiomyocyte apoptosis through the activator of transcription 3 (STAT3) signaling pathway [43]. In addition, STAT3 proteins played important roles in cancer cell survival and proliferation [44, 45]. Since CASR could activate the STAT3 pathway, and the activation of the STAT3 pathway promoted the development of drug resistance in ovarian cancer, we detected the STAT3 and p-STAT3 expression levels in vivo and in vitro experiments. We found that the expression level of p-STAT3 was negatively correlated with the expression level of CASR, which meant that CASR exerting as tumor suppressor may be achieved by inhibiting p-STAT3 in EOC cells, thereby promoting cell apoptosis and inhibiting cell proliferation. In this study, we verified that exosomal miR-429 secreted from SKOV3 cells enhanced DDP drug resistance in recipient cells via CASR/STAT3 in vivo.

According to the results of the transcription factor prediction analysis, we selected NF-κB for further research. NF-κB was the main transcription factor related to the induction of drug resistance. Moreover, in our experiments, the inhibition of NF-κB decreased the expression of miR-429 and the drug resistance of ovarian cancer cells. The NF-κB family consists of five related transcription factors: p50, p52, RelA (p65), c-Rel and RelB1,2. According to the predicted results, three possible binding sites for NF-κB were present in the miR-429 promoter region. NF-κB was a ubiquitous transcription factor that mediates cytoplasmic/nuclear signaling pathways [46]. A correlation has been identified between the activation of NF-κB and the control of apoptotic pathways, cell proliferation, differentiation, migration, angiogenesis, and resistance to chemotherapy/radiotherapy in tumor cells [47-50]. In particular, the overactivation of NF-κB led to resistance to standard chemotherapy agents, including PTX and DDP in OC [51, 52]. The inhibition of NF-κB decreased the expression of miR-429 and led to the sensitivity of OC cells. Additionally, A2780 cells cocultured with SKOV3 cells before treatment with the NF-κB inhibitor (PDTC) or miR-429 antagomir were sensitive to DDP and exhibited attenuated cell proliferation. In terms of inhibiting drug resistance, the inhibitory effect of NF-κB was greater than the miR-429-antagomir. We postulated that NF-κB might participate in the transcriptional regulation of multiple miRNAs. NF-κB was very likely to have a transcriptional regulatory effect on miR-429. Above all, NF-κB was very likely to have a transcriptional regulatory effect on miR-429.To further confirm this, we conducted a CHIP assay. According to the predicted three binding sites, we designed three pairs of primers: p65-chip-343, p65-chip-283, p65-chip-242, among which the enrichment efficiency of p65-chip-343 was more than 10 fold changes in SKOV3 and A2780 cells. The CHIP results supported that NF-κB had a transcriptional regulation effect on miR-429. NF-κB had several subunits, while p65 was the core subunit of transcription regulation, and it was in the predicted three NF-κB binding sites. Among the three predicted sites, two binding sites were RelA (p65), in addition, the antibody we used in the CHIP experiment

was NF-κB-p65, so we thought that NF-κB-p65 could bind to the miR-429 promoter region, and promote miR-429 transcription.

In our study, the mechanism of that NF-κB regulated miR-429 transcription and the identification of other downstream factors that conferred the drug resistance effect of miR-429 require further investigation. Overall, our current results indicated that DDP resistance was conferred by the horizontal transfer of exosomal miR-429 that subsequently inhibits CASR expression in EOC. Exosomal miR-429 might be a novel therapeutic target for EOC.

Acknowledgements

This research was supported by the Natural Science Foundation of China (Grant Nos. 81672913 and 81871343), the Social Development Project of Jiangsu (Grant Nos. BE2018693 and BE2017698), the Natural Science Foundation of Jiangsu Province (Grant No. BK20181226 and BK20201223), and Jiangsu Provincial Medical Youth Talent (Grant Nos. FRC201788 and QNRC2016460).

Disclosure of conflict of interest

None.

Address correspondence to: Dr. Xiaolan Zhu, Department of Central Laboratory, Reproductive Medicine Center, The Fourth Affiliated Hospital of Jiangsu University. No. 20 Zhengdong Road, Zhenjiang 212001, Jiangsu Province, China. E-mail: zxl2517@163.com

References

[1] Lisio MA, Fu L, Goyeneche A, Gao ZH and Telleria C. High-grade serous ovarian cancer: basic sciences, clinical and therapeutic standpoints. Int J Mol Sci 2019; 20: 952.

[2] Huang CY, Cheng M, Lee NR, Huang HY, Lee WL, Chang WH and Wang PH. Comparing paclitaxel-carboplatin with paclitaxel-cisplatin as the front-line chemotherapy for patients with figo iiic serous-type tubo-ovarian cancer. Int J Environ Res Public Health 2020; 17: 2213.

[3] Coleridge SL, Bryant A, Lyons TJ, Goodall RJ, Kehoe S and Morrison J. Chemotherapy versus surgery for initial treatment in advanced ovarian epithelial cancer. Cochrane Database Syst Rev 2019; 2019: CD005343.

[4] Mansoori B, Mohammadi A, Davudian S, Shirjang S and Baradaran B. The different mechanisms of cancer drug resistance: a brief review. Adv Pharm Bull 2017; 7: 339-348.

[5] Kowal J, Tkach M and Thery C. Biogenesis and secretion of exosomes. Curr Opin Cell Biol 2014; 29: 116-125.

[6] Xavier CPR, Caires HR, Barbosa MAG, Bergantim R, Guimaraes JE and Vasconcelos MH. The role of extracellular vesicles in the hallmarks of cancer and drug resistance. Cells 2020; 9: 1141.

[7] Valadi H, Ekstrom K, Bossios A, Sjostrand M, Lee JJ and Lotvall JO. Exosome-mediated transfer of mRNAs and microRNAs is a novel mechanism of genetic exchange between cells. Nat Cell Biol 2007; 9: 654-659.

[8] Mao L, Li J, Chen WX, Cai YQ, Yu DD, Zhong SL, Zhao JH, Zhou JW and Tang JH. Exosomes decrease sensitivity of breast cancer cells to adriamycin by delivering microRNAs. Tumour Biol 2016; 37: 5247-5256.

[9] Marabini R, Sirtori P, Chionna R, Barzizza L and Rubinacci A. Galactosylhydroxylysine and pyridinium cross links in monitoring the bone response to hormone replacement therapy. J Endocrinol Invest 1996; 19: 154-158.

[10] Yu DD, Wu Y, Zhang XH, Lv MM, Chen WX, Chen X, Yang SJ, Shen H, Zhong SL, Tang JH and Zhao JH. Exosomes from adriamycin-resistant breast cancer cells transmit drug resistance partly by delivering miR-222. Tumour Biol 2016; 37: 3227-3235.

[11] Liu X, Lu Y, Xu Y, Hou S, Huang J, Wang B, Zhao J, Xia S, Fan S, Yu X, Du Y, Hou L, Li Z, Ding Z, An S, Huang B, Li L, Tang J, Ju J, Guan H and Song B. Exosomal transfer of miR-501 confers doxorubicin resistance and tumorigenesis via targeting of BLID in gastric cancer. Cancer Lett 2019; 459: 122-134.

[12] Fu X, Liu M, Qu S, Ma J, Zhang Y, Shi T, Wen H, Yang Y, Wang S, Wang J, Nan K, Yao Y and Tian T. Exosomal microRNA-32-5p induces multidrug resistance in hepatocellular carcinoma via the PI3K/Akt pathway. J Exp Clin Cancer Res 2018; 37: 52.

[13] Wei F, Ma C, Zhou T, Dong X, Luo Q, Geng L, Ding L, Zhang Y, Zhang L, Li N, Li Y and Liu Y. Exosomes derived from gemcitabine-resistant cells transfer malignant phenotypic traits via delivery of miRNA-222-3p. Mol Cancer 2017; 16: 132.

[14] O'Brien J, Hayder H, Zayed Y and Peng C. Overview of microRNA biogenesis, mechanisms of actions, and circulation. Front Endocrinol (Lausanne) 2018; 9: 402.

[15] Oliveto S, Mancino M, Manfrini N and Biffo S. Role of microRNAs in translation regulation and cancer. World J Biol Chem 2017; 8: 45-56.

[16] Valinezhad Orang A, Safaralizadeh R and Kazemzadeh-Bavili M. Mechanisms of miRNA-

mediated gene regulation from common downregulation to mRNA-specific upregulation. Int J Genomics 2014; 2014: 970607.
[17] Peter ME. Targeting of mRNAs by multiple miRNAs: the next step. Oncogene 2010; 29: 2161-2164.
[18] Shivdasani RA. MicroRNAs: regulators of gene expression and cell differentiation. Blood 2006; 108: 3646-3653.
[19] Das S, Clezardin P, Kamel S, Brazier M and Mentaverri R. The CaSR in pathogenesis of breast cancer: a new target for early stage bone metastases. Front Oncol 2020; 10: 69.
[20] Diaz-Soto G, Rocher A, Garcia-Rodriguez C, Nunez L and Villalobos C. The calcium-sensing receptor in health and disease. Int Rev Cell Mol Biol 2016; 327: 321-369.
[21] Singh N, Promkan M, Liu G, Varani J and Chakrabarty S. Role of calcium sensing receptor (CaSR) in tumorigenesis. Best Pract Res Clin Endocrinol Metab 2013; 27: 455-463.
[22] Pfisterer J, Shannon CM, Baumann K, Rau J, Harter P, Joly F, Sehouli J, Canzler U, Schmalfeldt B, Dean AP, Hein A, Zeimet AG, Hanker LC, Petit T, Marmé F, El-Balat A, Glasspool R, de Gregorio N, Mahner S, Meniawy TM, Park-Simon TW, Mouret-Reynier MA, Costan C, Meier W, Reinthaller A, Goh JC, L'Haridon T, Baron Hay S, Kommoss S, du Bois A and Kurtz JE; AGO-OVAR 2.21/ENGOT-ov 18 Investigators. Bevacizumab and platinum-based combinations for recurrent ovarian cancer: a randomised, open-label, phase 3 trial. Lancet Oncol 2020; 21: 699-709.
[23] Pokhriyal R, Hariprasad R, Kumar L and Hariprasad G. Chemotherapy resistance in advanced ovarian cancer patients. Biomark Cancer 2019; 11: 1179299X19860815.
[24] Carretero-Gonzalez A, Otero I, Carril-Ajuria L, de Velasco G and Manso L. Exosomes: definition, role in tumor development and clinical implications. Cancer Microenviron 2018; 11: 13-21.
[25] Guo W, Li Y, Pang W and Shen H. Exosomes: a potential therapeutic tool targeting communications between tumor cells and macrophages. Mol Ther 2020; 28: 1953-1964.
[26] Maia J, Caja S, Strano Moraes MC, Couto N and Costa-Silva B. Exosome-based cell-cell communication in the tumor microenvironment. Front Cell Dev Biol 2018; 6: 18.
[27] Zhao L, Yu J, Wang J, Li H, Che J and Cao B. Isolation and Identification of miRNAs in exosomes derived from serum of colon cancer patients. J Cancer 2017; 8: 1145-1152.
[28] Ingenito F, Roscigno G, Affinito A, Nuzzo S, Scognamiglio I, Quintavalle C and Condorelli G. The role of exo-miRNAs in cancer: a focus on therapeutic and diagnostic applications. Int J Mol Sci 2019; 20: 4687.
[29] Sempere LF, Keto J and Fabbri M. Exosomal microRNAs in breast cancer towards diagnostic and therapeutic applications. Cancers (Basel) 2017; 9: 71.
[30] Bach DH, Hong JY, Park HJ and Lee SK. The role of exosomes and miRNAs in drug-resistance of cancer cells. Int J Cancer 2017; 141: 220-230.
[31] Yang Z, Zhao N, Cui J, Wu H, Xiong J and Peng T. Exosomes derived from cancer stem cells of gemcitabine-resistant pancreatic cancer cells enhance drug resistance by delivering miR-210. Cell Oncol (Dordr) 2020; 43: 123-136.
[32] Zhang HD, Jiang LH, Hou JC, Zhong SL, Zhu LP, Wang DD, Zhou SY, Yang SJ, Wang JY, Zhang Q, Xu HZ, Zhao JH, Ji ZL and Tang JH. Exosome: a novel mediator in drug resistance of cancer cells. Epigenomics 2018; 10: 1499-1509.
[33] Jin J, Tang S, Xia L, Du R, Xie H, Song J, Fan R, Bi Q, Chen Z, Yang G, Liu J, Shi Y and Fan D. MicroRNA-501 promotes HBV replication by targeting HBXIP. Biochem Biophys Res Commun 2013; 430: 1228-1233.
[34] Guo C, Zhao D, Zhang Q, Liu S and Sun MZ. miR-429 suppresses tumor migration and invasion by targeting CRKL in hepatocellular carcinoma via inhibiting Raf/MEK/ERK pathway and epithelial-mesenchymal transition. Sci Rep 2018; 8: 2375.
[35] Guo CM, Liu SQ and Sun MZ. miR-429 as biomarker for diagnosis, treatment and prognosis of cancers and its potential action mechanisms: a systematic literature review. Neoplasma 2020; 67: 215-228.
[36] Qiu M, Liang Z, Chen L, Tan G, Wang K, Liu L, Liu J and Chen H. MicroRNA-429 suppresses cell proliferation, epithelial-mesenchymal transition, and metastasis by direct targeting of BMI1 and E2F3 in renal cell carcinoma. Urol Oncol 2015; 33: 332, e9-18.
[37] Ye ZB, Ma G, Zhao YH, Xiao Y, Zhan Y, Jing C, Gao K, Liu ZH and Yu SJ. miR-429 inhibits migration and invasion of breast cancer cells in vitro. Int J Oncol 2015; 46: 531-538.
[38] Sheng N, Zhang L and Yang S. MicroRNA-429 decreases the invasion ability of gastric cancer cell line BGC-823 by downregulating the expression of heparanase. Exp Ther Med 2018; 15: 1927-1933.
[39] Dong H, Hao X, Cui B and Guo M. MiR-429 suppresses glioblastoma multiforme by targeting SOX2. Cell Biochem Funct 2017; 35: 260-268.
[40] Lin C, Huang F, Li QZ and Zhang YJ. miR-101 suppresses tumor proliferation and migration, and induces apoptosis by targeting EZH2 in esophageal cancer cells. Int J Clin Exp Pathol 2014; 7: 6543-6550.

[41] Deng Y, Luan F, Zeng L, Zhang Y and Ma K. MiR-429 suppresses the progression and metastasis of osteosarcoma by targeting ZEB1. EXCLI J 2017; 16: 618-627.
[42] Fan JY, Fan YJ, Wang XL, Xie H, Gao HJ, Zhang Y, Liu M and Tang H. miR-429 is involved in regulation of NF-kappaBactivity by targeting IKKbeta and suppresses oncogenic activity in cervical cancer cells. FEBS Lett 2017; 591: 118-128.
[43] Hong S, Zhang X, Zhang X, Liu W, Fu Y, Liu Y, Shi Z, Chi J, Zhao M and Yin X. Role of the calcium sensing receptor in cardiomyocyte apoptosis via mitochondrial dynamics in compensatory hypertrophied myocardium of spontaneously hypertensive rat. Biochem Biophys Res Commun 2017; 487: 728-733.
[44] Duan Z, Bradner JE, Greenberg E, Levine R, Foster R, Mahoney J and Seiden MV. SD-1029 inhibits signal transducer and activator of transcription 3 nuclear translocation. Clin Cancer Res 2006; 12: 6844-6852.
[45] Wen W, Wu J, Liu L, Tian Y, Buettner R, Hsieh MY, Horne D, Dellinger TH, Han ES, Jove R and Yim JH. Synergistic anti-tumor effect of combined inhibition of EGFR and JAK/STAT3 pathways in human ovarian cancer. Mol Cancer 2015; 14: 100.
[46] Wan F and Lenardo MJ. The nuclear signaling of NF-kappaB: current knowledge, new insights, and future perspectives. Cell Res 2010; 20: 24-33.
[47] Lehraiki A, Cerezo M, Rouaud F, Abbe P, Allegra M, Kluza J, Marchetti P, Imbert V, Cheli Y, Bertolotto C, Ballotti R and Rocchi S. Increased CD271 expression by the NF-kB pathway promotes melanoma cell survival and drives acquired resistance to BRAF inhibitor vemurafenib. Cell Discov 2015; 1: 15030.
[48] Valdes-Rives SA, Casique-Aguirre D, German-Castelan L, Velasco-Velazquez MA and Gonzalez-Arenas A. Apoptotic signaling pathways in glioblastoma and therapeutic implications. Biomed Res Int 2017; 2017: 7403747.
[49] Wang W, Nag SA and Zhang R. Targeting the NFkappaB signaling pathways for breast cancer prevention and therapy. Curr Med Chem 2015; 22: 264-289.
[50] Yang L, Shi P, Zhao G, Xu J, Peng W, Zhang J, Zhang G, Wang X, Dong Z, Chen F and Cui H. Targeting cancer stem cell pathways for cancer therapy. Signal Transduct Target Ther 2020; 5: 8.
[51] Cahill KE, Morshed RA and Yamini B. Nuclear factor-kappaB in glioblastoma: insights into regulators and targeted therapy. Neuro Oncol 2016; 18: 329-339.
[52] Oeckinghaus A and Ghosh S. The NF-kappaB family of transcription factors and its regulation. Cold Spring Harb Perspect Biol 2009; 1: a000034.

Table S1. Characteristics of NC and EOC patients

Characteristics	Age (years)	Gender	Pathological type	FIGO stage
NC 1	65	female	-	-
NC 2	62	female	-	-
NC 3	70	female	-	-
EOC 1	71	female	serous carcinoma	II
EOC 2	66	female	mucinous carcinoma	IV
EOC 3	64	female	endometrioid carcinoma	III

Table S2. Targetscan & miRanda & miRWalk-miRNA-mRNA-target gene prediction

miRNA	Accession Number	Gene Symbol	GeneID	Ensembl_Gene_ID
hsa-miR-429	MIMAT0001536	A1CF	29974	ENSG00000148584
hsa-miR-429	MIMAT0001536	AAK1	22848	ENSG00000115977
hsa-miR-429	MIMAT0001536	ABAT	18	ENSG00000183044
hsa-miR-429	MIMAT0001536	ABHD10	55347	ENSG00000144827
hsa-miR-429	MIMAT0001536	AFF4	27125	ENSG00000072364
hsa-miR-429	MIMAT0001536	AGFG1	3267	ENSG00000173744
hsa-miR-429	MIMAT0001536	AKAP6	9472	ENSG00000151320
hsa-miR-429	MIMAT0001536	AKT2	208	ENSG00000105221
hsa-miR-429	MIMAT0001536	AP1M1	8907	ENSG00000072958
hsa-miR-429	MIMAT0001536	AP1S2	8905	ENSG00000182287
hsa-miR-429	MIMAT0001536	ARPP21	10777	ENSG00000172995
hsa-miR-429	MIMAT0001536	ATP8A1	10396	ENSG00000124406
hsa-miR-429	MIMAT0001536	ATXN1	6310	ENSG00000124788
hsa-miR-429	MIMAT0001536	B3GALT1	8708	ENSG00000172318
hsa-miR-429	MIMAT0001536	C17orf51	339263	ENSG00000212719
hsa-miR-429	MIMAT0001536	C2orf69	205327	ENSG00000178074
hsa-miR-429	MIMAT0001536	CA5B	11238	ENSG00000169239
hsa-miR-429	MIMAT0001536	CACNA2D1	781	ENSG00000153956
hsa-miR-429	MIMAT0001536	CACNB2	783	ENSG00000165995
hsa-miR-429	MIMAT0001536	CACUL1	143384	ENSG00000151893
hsa-miR-429	MIMAT0001536	CASR	846	ENSG00000036828
hsa-miR-429	MIMAT0001536	CD274	29126	ENSG00000120217
hsa-miR-429	MIMAT0001536	CD59	966	ENSG00000085063
hsa-miR-429	MIMAT0001536	CDH11	1009	ENSG00000140937
hsa-miR-429	MIMAT0001536	CEP57L1	285753	ENSG00000183137
hsa-miR-429	MIMAT0001536	CHD2	1106	ENSG00000173575
hsa-miR-429	MIMAT0001536	CHRDL1	91851	ENSG00000101938
hsa-miR-429	MIMAT0001536	CHST11	50515	ENSG00000171310
hsa-miR-429	MIMAT0001536	CHST7	56548	ENSG00000147119
hsa-miR-429	MIMAT0001536	CLDND1	56650	ENSG00000080822
hsa-miR-429	MIMAT0001536	CNST	163882	ENSG00000162852
hsa-miR-429	MIMAT0001536	COMMD3	23412	ENSG00000148444
hsa-miR-429	MIMAT0001536	CRHBP	1393	ENSG00000145708
hsa-miR-429	MIMAT0001536	CUX1	1523	ENSG00000257923
hsa-miR-429	MIMAT0001536	CYTH3	9265	ENSG00000008256
hsa-miR-429	MIMAT0001536	DDIT4L	115265	ENSG00000145358
hsa-miR-429	MIMAT0001536	DDX3Y	8653	ENSG00000067048
hsa-miR-429	MIMAT0001536	DGKH	160851	ENSG00000102780

hsa-miR-429	MIMAT0001536	DOCK4	9732	ENSG00000128512
hsa-miR-429	MIMAT0001536	DUSP3	1845	ENSG00000108861
hsa-miR-429	MIMAT0001536	EGLN1	54583	ENSG00000135766
hsa-miR-429	MIMAT0001536	EIF1AX	1964	ENSG00000173674
hsa-miR-429	MIMAT0001536	EIF4B	1975	ENSG00000063046
hsa-miR-429	MIMAT0001536	EIF5	1983	ENSG00000100664
hsa-miR-429	MIMAT0001536	ELAVL4	1996	ENSG00000162374
hsa-miR-429	MIMAT0001536	ELK4	2005	ENSG00000158711
hsa-miR-429	MIMAT0001536	ELL	8178	ENSG00000105656
hsa-miR-429	MIMAT0001536	EPDR1	54749	ENSG00000086289
hsa-miR-429	MIMAT0001536	EVI5	7813	ENSG00000067208
hsa-miR-429	MIMAT0001536	FAM117B	150864	ENSG00000138439
hsa-miR-429	MIMAT0001536	FAM84A	151354	ENSG00000162981
hsa-miR-429	MIMAT0001536	FER	2241	ENSG00000151422
hsa-miR-429	MIMAT0001536	FOPNL	123811	ENSG00000133393
hsa-miR-429	MIMAT0001536	FZD4	8322	ENSG00000174804
hsa-miR-429	MIMAT0001536	GAB1	2549	ENSG00000109458
hsa-miR-429	MIMAT0001536	GAS2L3	283431	ENSG00000139354
hsa-miR-429	MIMAT0001536	GJC1	10052	ENSG00000182963
hsa-miR-429	MIMAT0001536	GOT1	2805	ENSG00000120053
hsa-miR-429	MIMAT0001536	GPR107	57720	ENSG00000148358
hsa-miR-429	MIMAT0001536	GPR137C	283554	ENSG00000180998
hsa-miR-429	MIMAT0001536	GPR180	160897	ENSG00000152749
hsa-miR-429	MIMAT0001536	GRAMD1B	57476	ENSG00000023171
hsa-miR-429	MIMAT0001536	HCCS	3052	ENSG00000004961
hsa-miR-429	MIMAT0001536	HEBP2	23593	ENSG00000051620
hsa-miR-429	MIMAT0001536	HIPK1	204851	ENSG00000163349
hsa-miR-429	MIMAT0001536	HSPA4L	22824	ENSG00000164070
hsa-miR-429	MIMAT0001536	ICA1L	130026	ENSG00000163596
hsa-miR-429	MIMAT0001536	IFIT5	24138	ENSG00000152778
hsa-miR-429	MIMAT0001536	IP6K1	9807	ENSG00000176095
hsa-miR-429	MIMAT0001536	IPO9	55705	ENSG00000198700
hsa-miR-429	MIMAT0001536	ITGA10	8515	ENSG00000143127
hsa-miR-429	MIMAT0001536	KBTBD6	89890	ENSG00000165572
hsa-miR-429	MIMAT0001536	KCNH5	27133	ENSG00000140015
hsa-miR-429	MIMAT0001536	KCNN3	3782	ENSG00000143603
hsa-miR-429	MIMAT0001536	KIAA0895	23366	ENSG00000164542
hsa-miR-429	MIMAT0001536	KIAA0930	23313	ENSG00000100364
hsa-miR-429	MIMAT0001536	KLHL14	57565	ENSG00000197705
hsa-miR-429	MIMAT0001536	KLHL42	57542	ENSG00000087448
hsa-miR-429	MIMAT0001536	KPNA6	23633	ENSG00000025800
hsa-miR-429	MIMAT0001536	KRR1	11103	ENSG00000111615
hsa-miR-429	MIMAT0001536	KRT80	144501	ENSG00000167767
hsa-miR-429	MIMAT0001536	LEPROTL1	23484	ENSG00000104660
hsa-miR-429	MIMAT0001536	LONRF2	164832	ENSG00000170500
hsa-miR-429	MIMAT0001536	LSM8	51691	ENSG00000128534
hsa-miR-429	MIMAT0001536	MAGOHB	55110	ENSG00000111196
hsa-miR-429	MIMAT0001536	MAN2A1	4124	ENSG00000112893
hsa-miR-429	MIMAT0001536	MAPK1IP1L	93487	ENSG00000168175
hsa-miR-429	MIMAT0001536	MAPKAPK5	8550	ENSG00000089022

hsa-miR-429	MIMAT0001536	MEGF10	84466	ENSG00000145794
hsa-miR-429	MIMAT0001536	MGEA5	10724	ENSG00000198408
hsa-miR-429	MIMAT0001536	MIB1	57534	ENSG00000101752
hsa-miR-429	MIMAT0001536	MIER1	57708	ENSG00000198160
hsa-miR-429	MIMAT0001536	MKLN1	4289	ENSG00000128585
hsa-miR-429	MIMAT0001536	MOCS2	4338	ENSG00000164172
hsa-miR-429	MIMAT0001536	MPC1	51660	ENSG00000060762
hsa-miR-429	MIMAT0001536	MPP7	143098	ENSG00000150054
hsa-miR-429	MIMAT0001536	MRAS	22808	ENSG00000158186
hsa-miR-429	MIMAT0001536	MTF2	22823	ENSG00000143033
hsa-miR-429	MIMAT0001536	N4BP2	55728	ENSG00000078177
hsa-miR-429	MIMAT0001536	NAA30	122830	ENSG00000139977
hsa-miR-429	MIMAT0001536	NAMPT	10135	ENSG00000105835
hsa-miR-429	MIMAT0001536	NCAPG2	54892	ENSG00000146918
hsa-miR-429	MIMAT0001536	NECTIN4	81607	ENSG00000143217
hsa-miR-429	MIMAT0001536	NOVA1	4857	ENSG00000139910
hsa-miR-429	MIMAT0001536	NPNT	255743	ENSG00000168743
hsa-miR-429	MIMAT0001536	OSBPL6	114880	ENSG00000079156
hsa-miR-429	MIMAT0001536	P2RX7	5027	ENSG00000089041
hsa-miR-429	MIMAT0001536	PCDH10	57575	ENSG00000138650
hsa-miR-429	MIMAT0001536	PCSK1	5122	ENSG00000175426
hsa-miR-429	MIMAT0001536	PCSK5	5125	ENSG00000099139
hsa-miR-429	MIMAT0001536	PDHA1	5160	ENSG00000131828
hsa-miR-429	MIMAT0001536	PEAK1	79834	ENSG00000173517
hsa-miR-429	MIMAT0001536	PIN4	5303	ENSG00000102309
hsa-miR-429	MIMAT0001536	PLEKHA3	65977	ENSG00000116095
hsa-miR-429	MIMAT0001536	PLPPR4	9890	ENSG00000117600
hsa-miR-429	MIMAT0001536	PPP2R2C	5522	ENSG00000074211
hsa-miR-429	MIMAT0001536	PRDM16	63976	ENSG00000142611
hsa-miR-429	MIMAT0001536	PTAR1	375743	ENSG00000188647
hsa-miR-429	MIMAT0001536	PTGER3	5733	ENSG00000050628
hsa-miR-429	MIMAT0001536	RAB21	23011	ENSG00000080371
hsa-miR-429	MIMAT0001536	RALGPS2	55103	ENSG00000116191
hsa-miR-429	MIMAT0001536	RBM3	5935	ENSG00000102317
hsa-miR-429	MIMAT0001536	RBM46	166863	ENSG00000151962
hsa-miR-429	MIMAT0001536	RDX	5962	ENSG00000137710
hsa-miR-429	MIMAT0001536	REPS2	9185	ENSG00000169891
hsa-miR-429	MIMAT0001536	RFTN1	23180	ENSG00000131378
hsa-miR-429	MIMAT0001536	RIMS2	9699	ENSG00000176406
hsa-miR-429	MIMAT0001536	RIMS3	9783	ENSG00000117016
hsa-miR-429	MIMAT0001536	RNF24	11237	ENSG00000101236
hsa-miR-429	MIMAT0001536	RUFY2	55680	ENSG00000204130
hsa-miR-429	MIMAT0001536	RUNDC1	146923	ENSG00000198863
hsa-miR-429	MIMAT0001536	RUNX1	861	ENSG00000159216
hsa-miR-429	MIMAT0001536	RWDD2A	112611	ENSG00000013392
hsa-miR-429	MIMAT0001536	SCML1	6322	ENSG00000047634
hsa-miR-429	MIMAT0001536	SEPT6	23157	ENSG00000125354
hsa-miR-429	MIMAT0001536	SESN3	143686	ENSG00000149212
hsa-miR-429	MIMAT0001536	SESTD1	91404	ENSG00000187231

hsa-miR-429	MIMAT0001536	SH3PXD2A	9644	ENSG00000107957
hsa-miR-429	MIMAT0001536	SHCBP1	79801	ENSG00000171241
hsa-miR-429	MIMAT0001536	SLAIN1	122060	ENSG00000139737
hsa-miR-429	MIMAT0001536	SLC16A2	6567	ENSG00000147100
hsa-miR-429	MIMAT0001536	SLC23A2	9962	ENSG00000089057
hsa-miR-429	MIMAT0001536	SLC25A30	253512	ENSG00000174032
hsa-miR-429	MIMAT0001536	SLC2A14	144195	ENSG00000173262
hsa-miR-429	MIMAT0001536	SLC2A3	6515	ENSG00000059804
hsa-miR-429	MIMAT0001536	SLC38A4	55089	ENSG00000139209
hsa-miR-429	MIMAT0001536	SLC4A8	9498	ENSG00000050438
hsa-miR-429	MIMAT0001536	SLCO4C1	353189	ENSG00000173930
hsa-miR-429	MIMAT0001536	SLF2	55719	ENSG00000119906
hsa-miR-429	MIMAT0001536	SLK	9748	ENSG00000065613
hsa-miR-429	MIMAT0001536	SMARCD1	6602	ENSG00000066117
hsa-miR-429	MIMAT0001536	SNTB2	6645	ENSG00000168807
hsa-miR-429	MIMAT0001536	SNX29	92017	ENSG00000048471
hsa-miR-429	MIMAT0001536	SOCS5	9655	ENSG00000171150
hsa-miR-429	MIMAT0001536	SOWAHC	65124	ENSG00000198142
hsa-miR-429	MIMAT0001536	SPATS2L	26010	ENSG00000196141
hsa-miR-429	MIMAT0001536	SREK1IP1	285672	ENSG00000153006
hsa-miR-429	MIMAT0001536	SRP72	6731	ENSG00000174780
hsa-miR-429	MIMAT0001536	ST3GAL5	8869	ENSG00000115525
hsa-miR-429	MIMAT0001536	STRN	6801	ENSG00000115808
hsa-miR-429	MIMAT0001536	SYCP2L	221711	ENSG00000153157
hsa-miR-429	MIMAT0001536	SYT1	6857	ENSG00000067715
hsa-miR-429	MIMAT0001536	TAF12	6883	ENSG00000120656
hsa-miR-429	MIMAT0001536	TAF5L	27097	ENSG00000135801
hsa-miR-429	MIMAT0001536	TBL1XR1	79718	ENSG00000177565
hsa-miR-429	MIMAT0001536	TCF4	6925	ENSG00000196628
hsa-miR-429	MIMAT0001536	TFAM	7019	ENSG00000108064
hsa-miR-429	MIMAT0001536	TFE3	7030	ENSG00000068323
hsa-miR-429	MIMAT0001536	TMEM100	55273	ENSG00000166292
hsa-miR-429	MIMAT0001536	TMEM17	200728	ENSG00000186889
hsa-miR-429	MIMAT0001536	TMEM26	219623	ENSG00000196932
hsa-miR-429	MIMAT0001536	TMF1	7110	ENSG00000144747
hsa-miR-429	MIMAT0001536	TMOD2	29767	ENSG00000128872
hsa-miR-429	MIMAT0001536	TRA2B	6434	ENSG00000136527
hsa-miR-429	MIMAT0001536	ULK2	9706	ENSG00000083290
hsa-miR-429	MIMAT0001536	USF3	205717	ENSG00000176542
hsa-miR-429	MIMAT0001536	USP49	25862	ENSG00000164663
hsa-miR-429	MIMAT0001536	UTY	7404	ENSG00000183878
hsa-miR-429	MIMAT0001536	VAT1L	57687	ENSG00000171724
hsa-miR-429	MIMAT0001536	VLDLR	7436	ENSG00000147852
hsa-miR-429	MIMAT0001536	WDFY2	115825	ENSG00000139668
hsa-miR-429	MIMAT0001536	ZBTB7C	201501	ENSG00000184828
hsa-miR-429	MIMAT0001536	ZBTB8B	728116	ENSG00000273274
hsa-miR-429	MIMAT0001536	ZFPM2	23414	ENSG00000169946
hsa-miR-429	MIMAT0001536	ZMAT3	64393	ENSG00000172667
hsa-miR-429	MIMAT0001536	ZNF148	7707	ENSG00000163848

Table S3. The prediction information of CASR in miRanda-miRNA-mRNA database

miRNA	Gene Symbol	Ensembl_Gene_ID	Transcript_ID	align_score	energy	miRNA_start	miRNA_end
hsa-miR-429	CASR	ENSG00000036828	ENST00000639785	175	-22.3	2	21
hsa-miR-429	CASR	ENSG00000036828	ENST00000638421	175	-22.3	2	21
hsa-miR-429	CASR	ENSG00000036828	ENST00000498619	175	-22.3	2	21

miRNA	gene_start	gene_end	miRNA_align	alignment	gene_align	Transcript_ID1
hsa-miR-429	766	788	3 ugCCAAA-AUGGUCUGUCAUAAu5	||||| ||: ||:|||||||	5ctGGTTTATATAAGGCAGTATTa3	ENST00000639785
hsa-miR-429	766	788	3 ugCCAAA-AUGGUCUGUCAUAAu5	||||| ||: ||:|||||||	5ctGGTTTATATAAGGCAGTATTa3	ENST00000638421
hsa-miR-429	766	788	3 ugCCAAA-AUGGUCUGUCAUAAu5	||||| ||: ||:|||||||	5ctGGTTTATATAAGGCAGTATTa3	ENST00000498619

Table S4. The prediction information of CASR in miRWalk-miRNA-mRNA database

miRNA	Transcript_ID	Gene Symbol	binding_site	binding_probability
hsa-miR-429	ENST00000639785	CASR	4375,4398	1
hsa-miR-429	ENST00000638421	CASR	4956,4979	1
hsa-miR-429	ENST00000498619	CASR	4471,4494	1
hsa-miR-429	ENST00000490131	CASR	4347,4370	1

Table S5. The prediction information of CASR in TargetScan-miRNA-mRNA database

miRNA	Accession Number	Gene Symbol	GeneID	Ensembl_Gene_ID	Transcript_ID	Site Type	TR start	TR end
hsa-miR-429	MIMAT0001536	CASR	846	ENSG00000036828	ENST00000498619	8mer-1a	781	788
miRNA	context + score	context + score percentile	TR region	TR-miRNA pairing	mature miRNA sequence			
hsa-miR-429	-0.906	94	UGGUUUAUAUAAGGCAGUAUUA	|||| |||||||	GCCAAAAUGGUCU--GUCAUAAU			

Table S6. MiR-429 transcription factor prediction results

Sequence name	Factor name	Start position	End position	Dissimilarity	String	RE equally	RE query
miR-429	GR [T05076]	1559	1571	8.240002	ACAAGAACAGGAA	0.00572	0.00231
miR-429	HNF-1C [T01951]	1714	1722	4.824832	ACTCATTAA	0.04578	0.00239
miR-429	E12 [T00204]	489	501	3.304512	CCCAGCAGGTGCG	0.00164	0.00329
miR-429	SF-1 [T02769]	1338	1348	5.584475	GTGACCTGGCT	0.00763	0.00555
miR-429	HNF-4alpha [T03828]	1567	1579	13.987389	AGGAACTTTGTCC	0.02396	0.00598
miR-429	Ik-1 [T02702]	1836	1848	4.748597	CCAGGTGCTGGGA	0.00313	0.00601
miR-429	LEF-1 [T02905]	931	938	6.176008	GTTCAAAG	0.03052	0.00699
miR-429	RAR-beta: RXR-alpha [T05420]	1422	1433	2.492665	GGGCTCCGTGGA	0.00215	0.00701
miR-429	RelA [T00594]	892	901	3.744303	GGATTTCCCA	0.01335	0.00858
miR-429	NERF-1a [T05021]	1450	1461	6.512578	CAGGAAGGACAA	0.0093	0.00922
miR-429	NERF-1a [T05021]	1736	1747	6.606569	CAGGAAGCCAGC	0.0093	0.00922
miR-429	Smad4 [T04292]	1958	1968	11.011499	CCCGCAGACAC	0.01287	0.01109
miR-429	TFII-I [T00824]	889	899	12.023404	GCTGGATTTCC	0.01526	0.0125
miR-429	NF-kappaB [T00590]	1352	1362	9.662495	GGAAAGGCCAT	0.01526	0.0129
miR-429	Smad4 [T04292]	916	926	11.653625	CTGTCTGGTAA	0.03433	0.01365
miR-429	RAR-alpha1 [T00719]	324	333	5.263926	GTGACCTTCG	0.02289	0.01511
miR-429	MAZ [T00490]	1284	1294	3.753679	CCCTCCCGGAG	0.00191	0.01569
miR-429	RAR-beta: RXR-alpha [T05420]	12	23	8.434402	TCCTCAGTGCCC	0.00954	0.01615
miR-429	EBF [T05427]	726	736	7.366048	GTCTCAGGGCC	0.01144	0.01623
miR-429	ERRalpha1 [T05682]	323	335	11.351203	CGTGACCTTCGGA	0.04318	0.01649
miR-429	ERRalpha1 [T05682]	932	944	12.222268	TTCAAAGGTGACC	0.02879	0.01746
miR-429	RXR-alpha [T01345]	325	333	0.685729	TGACCTTCG	0.04578	0.01832
miR-429	RORalpha1 [T01527]	1339	1348	4.458228	TGACCTGGCT	0.03433	0.01874
miR-429	Ik-1 [T02702]	1360	1372	7.122895	CATAGGGCTGGGA	0.01064	0.01977
miR-429	IA-1 [T05887]	1672	1684	7.881783	GGGGAGGGGGCAG	0.00358	0.01986
miR-429	E12 [T00204]	1912	1924	13.208774	TGCAGGAGGTGGC	0.00995	0.02042
miR-429	IA-1 [T05887]	332	344	7.411963	CGGAAGGGGGCTG	0.00489	0.02203
miR-429	GABP [T00268]	330	341	8.320539	TTCGGAAGGGGG	0.00858	0.02219
miR-429	Tal-1 [T00790]	440	450	7.076519	CAGGTGTCCGG	0.02766	0.02323
miR-429	PU.1 [T02068]	696	705	3.671499	GAGGAAGCAG	0.0267	0.02389
miR-429	T3R-alpha [T00838]	1593	1604	10.42539	CCAGGATGACCC	0.03505	0.02414
miR-429	EBF [T05427]	804	814	8.844893	TTCCCTGGGCT	0.01526	0.02509
miR-429	Pbx1b [T02087]	1205	1214	6.962606	TCACTCACGC	0.03052	0.02572

miR-429	FOXN2 [T04206]	694	704	5.570023	TGGAGGAAGCA	0.02575	0.02727
miR-429	E2F-1: DP-1 [T05204]	837	845	3.015334	TGGCGGGAC	0.00763	0.02785
miR-429	PKNOX1 [T04122]	1854	1864	5.212169	GCTGTCAGGGA	0.04292	0.02815
miR-429	Egr-3 [T00243]	1807	1819	9.828903	TACCCCCACACAG	0.02503	0.0296
miR-429	ELF-1 [T01113]	157	169	14.280835	ATACTGCCTGGTA	0.04911	0.02997
miR-429	GCMa [T02306]	1488	1496	7.538507	CATGCAGGG	0.02289	0.03009
miR-429	SF-1 [T02769]	324	334	7.358084	GTGACCTTCGG	0.0267	0.03136
miR-429	TFII-I [T00824]	992	1002	8.786263	CAGGGATGGGC	0.0391	0.0333
miR-429	T3R-beta1 [T00851]	146	156	10.266515	TCAGGTCTCTA	0.0329	0.03415
miR-429	ER-beta [T04651]	1339	1347	0.423191	TGACCTGGC	0.03052	0.03585
miR-429	AP-4 [T00036]	390	400	3.002248	CCTGCAGCTGC	0.01764	0.03602
miR-429	AP-4 [T00036]	1907	1917	3.002248	GCAGCTGCAGG	0.01764	0.03602
miR-429	RFX1 [T01673]	67	75	2.7576	CCATGCAAC	0.03052	0.03621
miR-429	CRF [T00170]	128	139	8.237356	GGGCAGCATTGG	0.02146	0.0372
miR-429	RelA [T00594]	50	59	5.93965	GAGCTTCCCA	0.03052	0.04167
miR-429	FOXN2 [T04206]	25	35	6.471094	AGGAGGACGAG	0.03433	0.04216
miR-429	PU.1 [T02068]	567	576	3.899853	GAGGAAGCCG	0.04005	0.04338
miR-429	EBF [T05427]	219	229	0.10398	CCCCCAGGGCC	0.00381	0.04393
miR-429	EBF [T05427]	1162	1172	0	CCCCCAGGGGA	0.00381	0.04393
miR-429	FOXN2 [T04206]	8	18	14.405409	GCTGTCCTCAG	0.03719	0.04827
miR-429	BTEB3 [T05051]	246	254	5.509757	ACTCCCCTC	0.03052	0.04834

Table S7. CHIP related primer sequence

Name	sequences 5'-3'
p65-chip-343-F1	GCCGGGATCACATTCCTC
p65-chip-343-R1	GTGGCCACAGGTCAAGAAAT
p65-chip-283-F2	AGGTGATGGAAAGGGAAAGC
p65-chip-283-R2	CAAGTTTTCTGGCACCTTCC
p65-chip-242-F3	GGGCCTTTGAGAAGAGAAGG
p65-chip-242-R3	CCGAGGACTAGGTCGGAGT

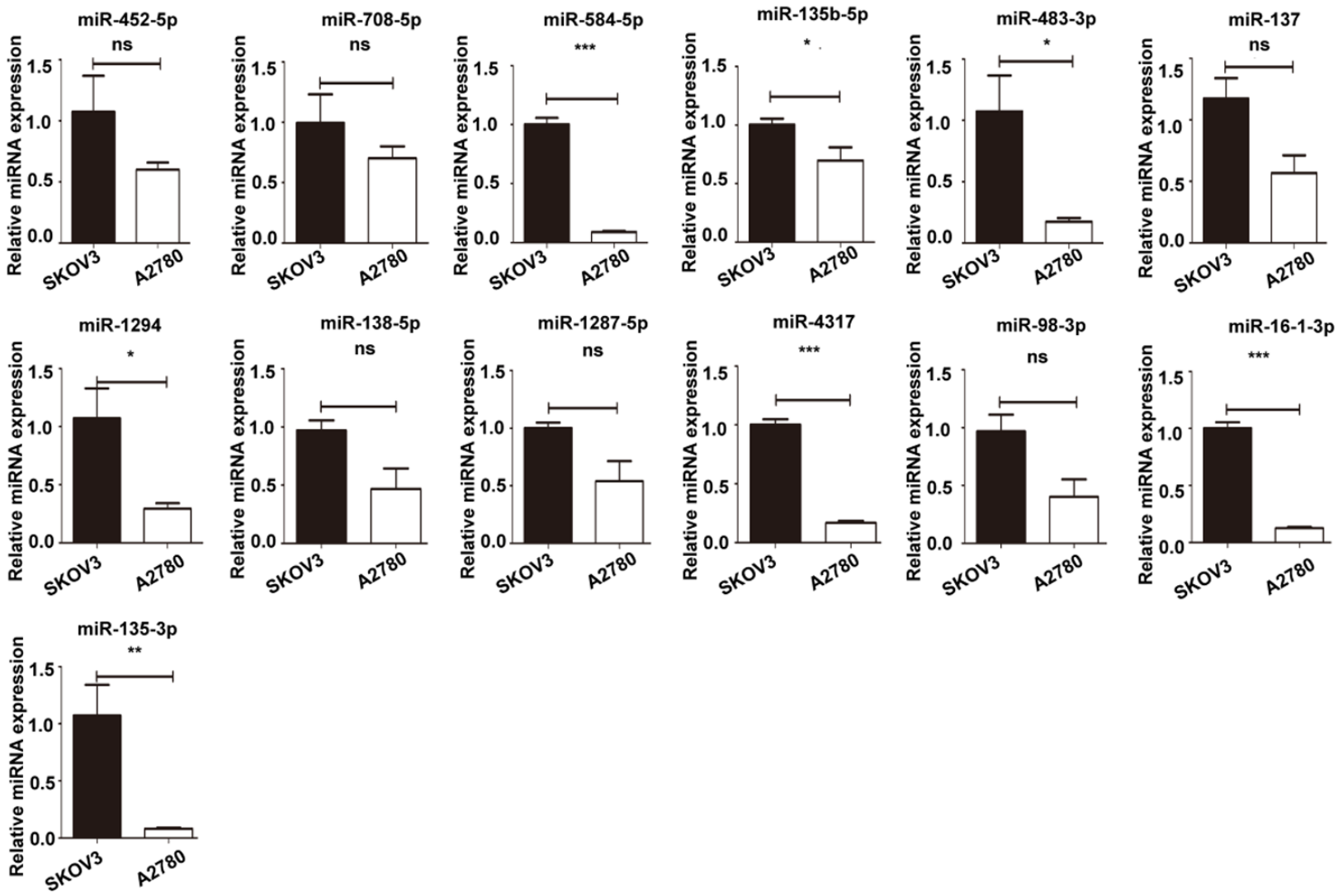
miR-452-5p
ns
miR-708-5p
ns
miR-584-5p
***
miR-135b-5p
*
miR-483-3p
*
miR-137
ns
miR-1294
*
miR-138-5p
ns
miR-1287-5p
ns
miR-4317
***
miR-98-3p
ns
miR-16-1-3p
***
miR-135-3p
**
Relative miRNA expression
1.5
1.0
0.5
0.0
SKOV3
A2780

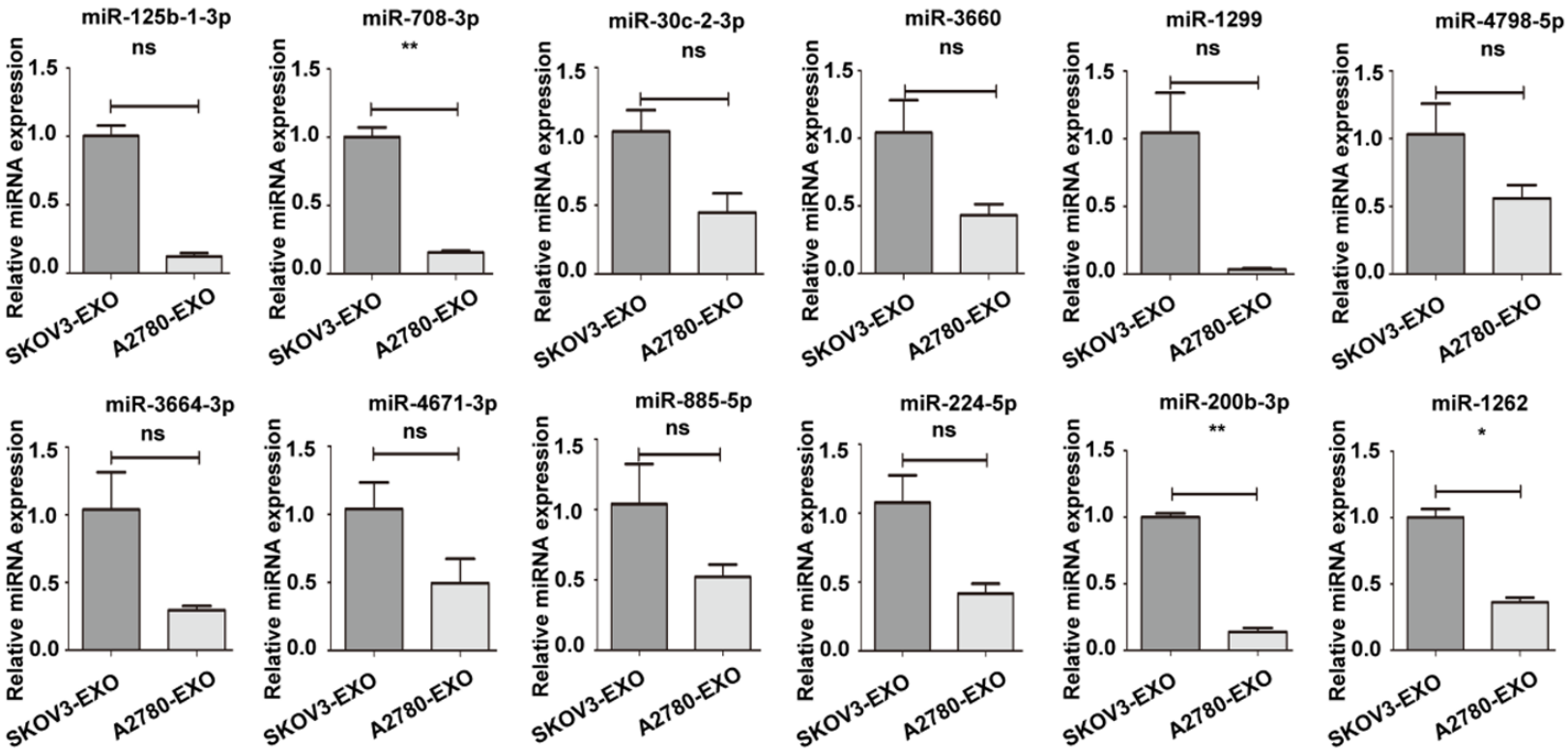

Figure S1. The verification results of the other 19 miRNAs expressed in SKOV3 cells higher than that in A2780 cells and the other 12 miRNAs that have higher expression in SKOV3-EXO than A2780-EXO.

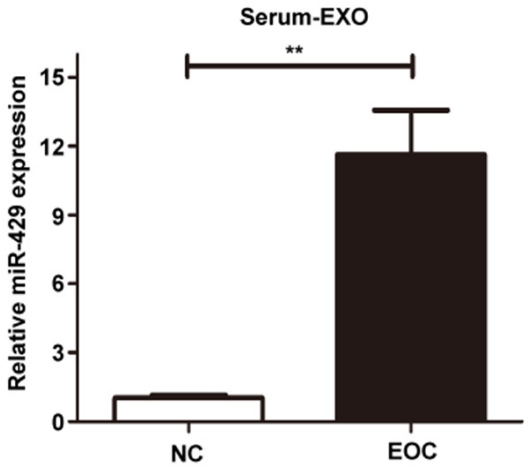

Figure S2. The expression of miR-429 in NC and EOC Serum-EXO.

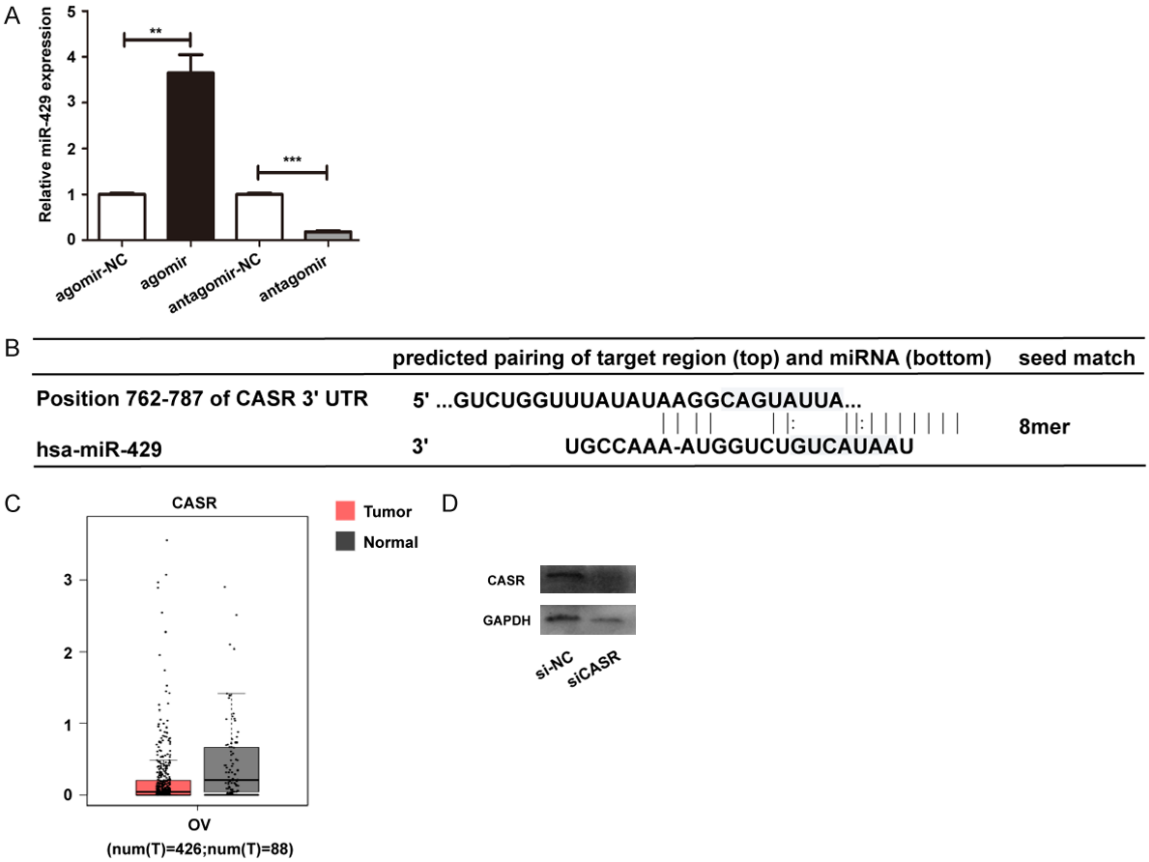

Figure S3. A. The infection efficiency of miR-429 was confirmed by real-time qRT-PCR. B. The predicted binding area of miR-429 and CASR in the Targetscan database. C. In the GEPIA database, the expression level of CASR in ovarian cancer tissues and normal ovarian tissues. D. The infection efficiency of si-CASR was confirmed by Western blot assay.

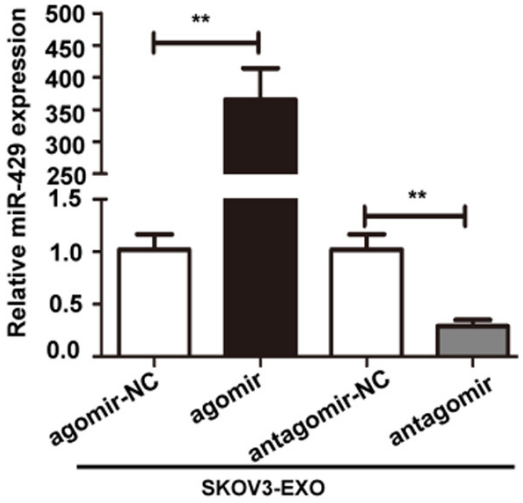

Figure S4. The infection efficiency of miR-429 in SKOV3-EXO was confirmed by real-time qRT-PCR.

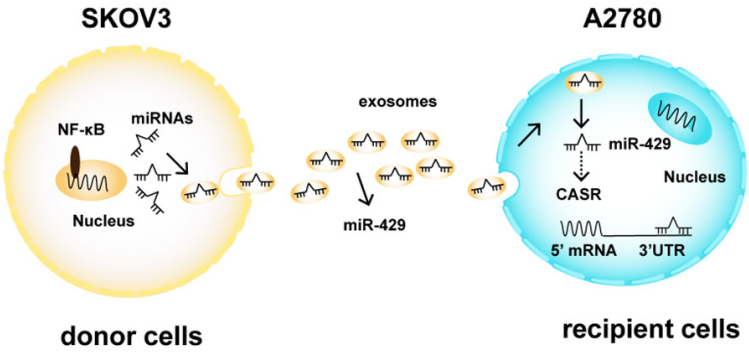

Figure S5. The schematic diagram for the underlying effects of exosomal miR-429 on EOC.

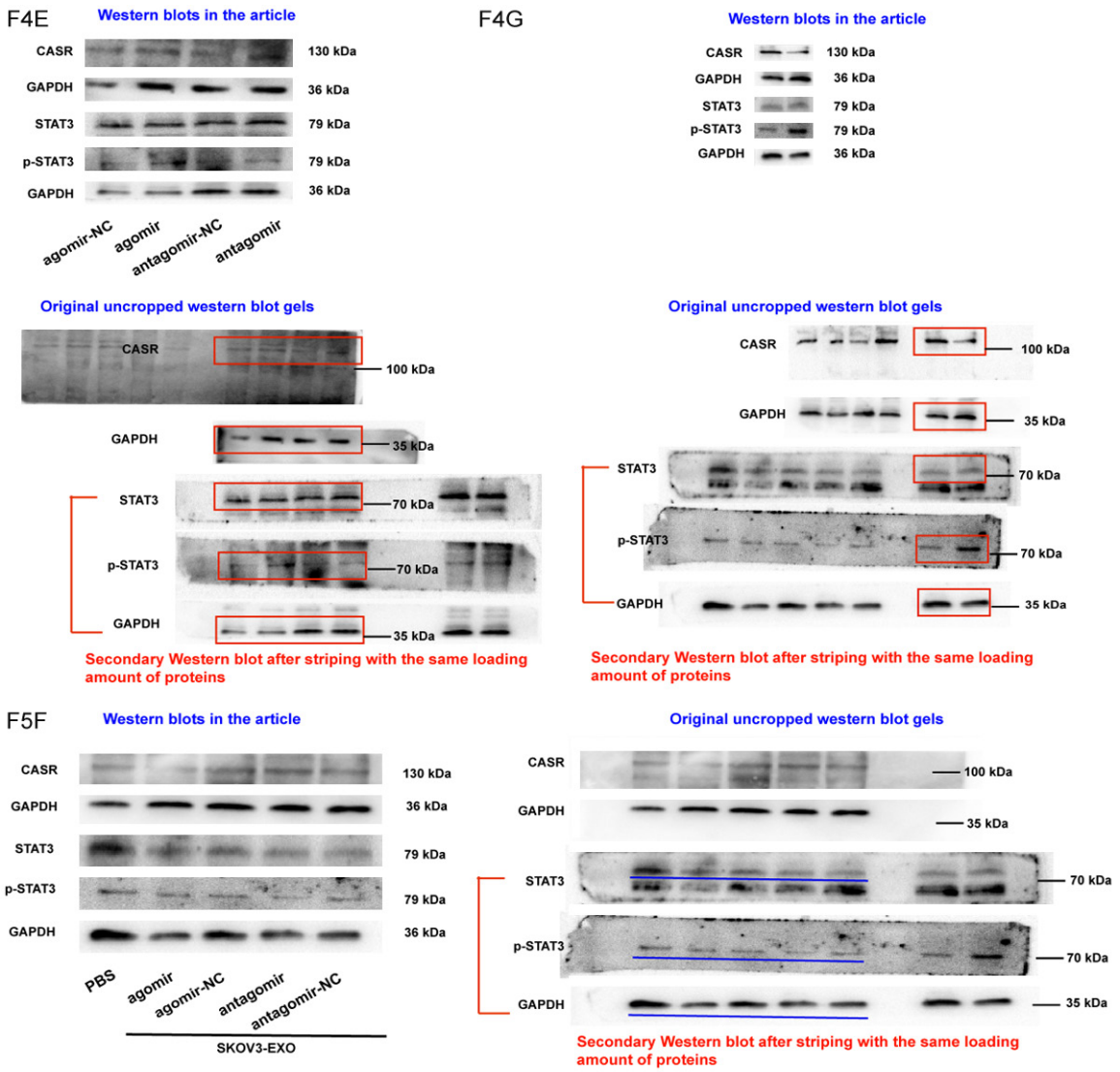

Figure S6. The original uncropped gels of **Figures 4E**, **4G**, **5F** for western blots.

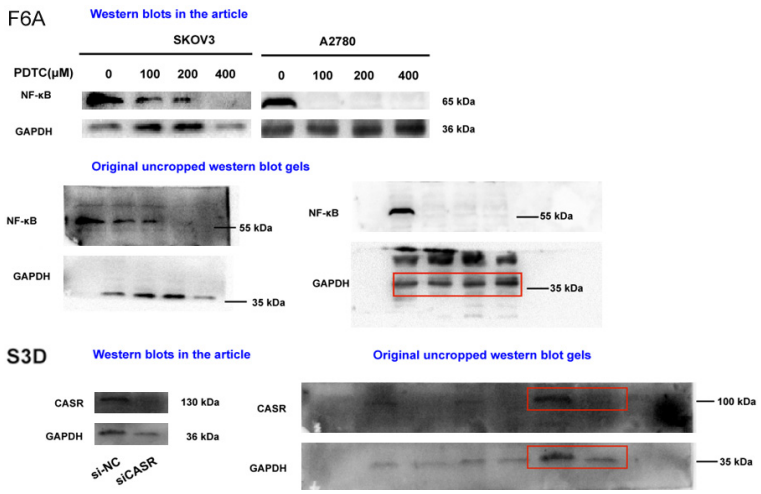

Figure S7. The original uncropped gels of **Figures 6A**, S3D for western blots.